

THEORETICAL BASE PRESSURE ANALYSIS OF  
AXISYMMETRIC EJECTORS WITHOUT INDUCED FLOW

By

R. C. Bauer

Rocket Test Facility

ARO, Inc.

a subsidiary of Sverdrup and Parcel, Inc.

January 1964

ARO Project No. RW2141

# *Contrails*

**FOREWORD**

The experimental data originating in this report were obtained by J. H. Panesci and R. C. German. Theoretical results were obtained from an IBM 7070 computer programmed by D. H. Hoyle.

# *Contrails*


**ABSTRACT**

The two-dimensional supersonic base pressure theory developed by Dr. H. H. Korst, which applies to two-dimensional systems with straight jet boundaries, has been modified to be more applicable to axisymmetric ejector systems. The modification consists of a new theory for estimating the peak recompression static pressure which is applicable to either axisymmetric or two-dimensional jets having straight or curved boundaries. Significantly, the recompression mechanism is not independent of viscous effects for systems which produce a non-uniform inviscid flow field.

Both the recompression theory and the modified base pressure theory are experimentally verified for the case of isoenergetic mixing and negligible initial boundary layer. The recompression theory is shown to agree with experimental results to within  $\pm 10$  percent, whereas the experimental base pressure results have a standard deviation of 6 percent with respect to the modified base pressure theory.

**PUBLICATION REVIEW**

**This report has been reviewed and publication is approved.**

  
Eules L. Hively  
Acting Chief, Propulsion Division  
DCS/Research

  
Donald R. Eastman, Jr.  
DCS/Research

# *Contrails*

CONTENTS

	<u>Page</u>
ABSTRACT. . . . .	v
NOMENCLATURE. . . . .	ix
1.0 INTRODUCTION . . . . .	1
2.0 RECOMPRESSION MECHANISM . . . . .	2
3.0 THEORETICAL MINIMUM CELL PRESSURE RATIO OF AXISYMMETRIC EJECTOR SYSTEMS . . . . .	12
4.0 CONCLUSIONS . . . . .	14
REFERENCES . . . . .	15

TABLES

1. Comparison of Theoretical with Experimental Peak Recompression Static Pressure. . . . .	17
2. Comparison of Theoretical with Experimental Minimum Cell Pressure Ratios of Axisymmetric Ejectors . . . . .	18

ILLUSTRATIONS

Figure

1. Sketch of a Typical Ejector System. . . . .	19
2. Sketch of Experimental Configurations	
a. Total Pressure Rake Installation. . . . .	20
b. Total Pressure Probe Installation . . . . .	20
3. Comparison of Theoretical with Experimental Lines of Constant Mach Number in a Free Jet, $A_{ne}/A^* = 10.848$ . . . . .	21
4. Comparison of Theoretical with Experimental Lines of Constant Mach Number in a Free Jet, $A_{ne}/A^* = 25.000$ . . . . .	22
5. Comparison of Theoretical with Experimental Measured Total Pressure in a Free Jet . . . . .	23

<u>Figure</u>		<u>Page</u>
6.	Theoretical Recompression Flow Field (First Order). . . . .	24
7.	$p_2/p_t$ vs $M$ - Two-Dimensional Shock Wave Theory. . .	25
8.	Typical Isentropic Compression and Expansion Processes . . . . .	26
9.	Typical Error of Approximation to Two-Dimensional Shock Wave Theory . . . . .	27
10.	Theoretical and Experimental Impingement Zone Characteristics	
	a. Inviscid Flow Conditions . . . . .	28
	b. Diffuser Wall Static Pressure Distribution. . . . .	28
11.	Theoretical and Experimental Impingement Zone Characteristics	
	a. Inviscid Flow Conditions. . . . .	29
	b. Diffuser Wall Static Pressure Distribution. . . . .	29
12.	Idealized Flow Phenomena at Impingement Point	
	a. Idealized Static Pressure Distribution. . . . .	30
	b. Idealized Flow Phenomena. . . . .	30
13.	Variation of Mixing Zone Characteristics with Crocco Number Squared. . . . .	31
14.	Comparison of Theoretical with Experimental Peak Recompression Static Pressure as a Function of $p_c/p_t$	
	a. $A_{ne}/A^* = 3.627$ . . . . .	32
	b. $A_{ne}/A^* = 10.848$ . . . . .	32
	c. $A_{ne}/A^* = 25.000$ . . . . .	33
15.	Comparison of Theoretical with Experimental Peak Recompression Static Pressure as a Function of Nozzle Total Pressure	
	a. $A_{ne}/A^* = 3.627$ . . . . .	34
	b. $A_{ne}/A^* = 10.848$ . . . . .	34
	c. $A_{ne}/A^* = 25.000$ . . . . .	35
16.	Comparison of Theoretical with Experimental Minimum Cell Pressure Ratios	
	a. Data from Ref. 7 . . . . .	36
	b. Data from Ref. 16 . . . . .	37
	c. Data from Ref. 4 . . . . .	38
	d. Data from Ref. 4 . . . . .	39
	e. Data from Ref. 4 . . . . .	40



**NOMENCLATURE**

$A^*$	Area of nozzle throat
$A_D$	Area of diffuser
$A_{ne}$	Area of nozzle exit (Fig. 1)
$b$	Width of mixing zone (Fig. 8b)
$C_{aj}$	Inviscid jet boundary Crocco number, $\sqrt{1 - T_j/T_t}$
$c$	Rate of growth of mixing zone
$k$	Location of mixing zone relative to inviscid jet boundary (Fig. 12)
$l_j$	Length along inviscid jet boundary from nozzle exit to diffuser wall
$M$	Mach number
$M_j$	Mach number of inviscid jet boundary
$p$	Static pressure
$p_c$	Base or cell pressure (Fig. 1)
$p_t$	Total pressure
$p_t'$	Total pressure downstream of a normal shock wave
$p_w$	Static pressure on diffuser wall
$r_D$	Radius of diffuser
$r_{ne}$	Radius of nozzle exit (Fig. 1)
$r_p$	Radius of total pressure probe (Fig. 2b)
$T_t$	Gas total temperature
$T_j$	Inviscid jet boundary static temperature
$u$	Velocity anywhere in mixing zone (Fig. 12b)
$u_\infty$	Velocity at inner edge of mixing zone (Fig. 12b)
$X$	Distance from nozzle exit plane parallel to nozzle centerline (Fig. 2)
$Y$	Distance perpendicular to nozzle centerline (Fig. 2)
$\beta$	Inviscid jet boundary recompression turning angle
$\gamma$	Ratio of specific heats

$\eta$	Non-dimensional mixing zone coordinate (Refs. 7, 8, and 9; Fig. 12b)
$\eta_M$	Non-dimensional location of inner edge of mixing zone (Fig. 12b)
$\eta_s$	Non-dimensional location of stagnating streamline (Fig. 12b)
$\eta_\infty$	Non-dimensional location of inviscid jet boundary (Fig. 12b)
$\theta_{ne}$	Nozzle exit wall angle relative to nozzle centerline

## SUBSCRIPTS

exp	Experimental
max	Maximum
min	Minimum
theo	Theoretical

## 1.0 INTRODUCTION

The ejector research program conducted in the Rocket Test Facility (RTF), Arnold Engineering Development Center (AEDC), Air Force Systems Command (AFSC), has been primarily of an experimental nature. The purpose of the overall research program is to define the various factors which influence the performance of axisymmetric ejector systems. The results are presented in Refs. 1 through 6. Based on these experimental results, simple empirical methods were developed for estimating the performance of axisymmetric ejector systems. In this report, the two-dimensional base pressure theory for isoenergetic mixing and negligible initial boundary layer, developed by Korst (Ref. 7), is extended to improve the applicability of this theory to predict the minimum cell pressure ratio produced by axisymmetric ejector systems.

The two-dimensional supersonic base pressure theory developed by Korst consists of two independent theories which, when solved simultaneously, yield the base pressure. The criterion for the simultaneous solution is that the total pressure on the dividing streamline in the mixing zone must equal the peak recompression static pressure in the impingement zone. In Ref. 7 these theories were developed for two-dimensional mixing along a uniform inviscid jet flow field. The total pressure on the dividing streamline in the mixing zone is determined by applying overall momentum and conservation of mass flow relations to the mixing zone using a velocity distribution derived by simplifying and solving the basic equations for turbulent flow. The peak recompression static pressure is determined by turning the inviscid flow field parallel to the impingement surface by means of a two-dimensional shock wave.

In Ref. 7 it is shown that, for axisymmetric ejector systems, Korst's two-dimensional supersonic base pressure theory predicts minimum cell pressure ratios greater than experimental values ( $1.60 < M_j < 3.50$ ) with the deviation increasing as the area ratio of the driving nozzle increases. The basic assumptions of the theory are reviewed (Ref. 8) with regard to their compatibility with the conditions that are produced by an axisymmetric ejector system. The results of that investigation of interest here are as follows:

1. The theoretical total pressure on the dividing streamline agrees with the measured peak recompression static pressure if it is assumed that the stagnation process is isentropic and that the mixing is two-dimensional.

---

Manuscript received December 1963.

2. The theoretical peak recompression static pressure obtained by applying two-dimensional shock wave theory based on a free-jet Mach number determined by the ratio  $p_c/p_t$  is shown to disagree seriously with the measured peak recompression static pressure.

These conclusions have also been experimentally verified by data obtained at the AEDC. In addition to the above-mentioned considerations, the axisymmetric effects on the characteristics of a mixing zone have been theoretically investigated in Refs. 8 and 9. Application of the theory presented in these references to the typical ejector systems studied in Refs. 1 through 6 shows that the axisymmetric effects on mixing are negligible for these systems.

The above discussion leads to the conclusion that the major source of error in the application of Korst's two-dimensional supersonic base pressure theory to axisymmetric ejector systems is in the method used for predicting the peak recompression pressure. An empirical method for estimating the peak recompression, based on relatively limited experimental data ( $2.57 < M_j < 3.41$ ), is presented in Ref. 8. The corrected base pressure theory is then shown to predict very accurately the minimum cell pressure ratio of a limited number of axisymmetric ejector systems. In this report, a theoretical method of estimating the peak recompression pressure is developed, and the modified base pressure theory is applied to a wide range of axisymmetric ejector systems ( $1.60 < M_j < 7.4$ ).

The recompression theory developed in this report is applicable to any system involving the impingement of a free jet on a solid surface.

## 2.0 RECOMPRESSION MECHANISM

The basic premise of this analysis is that the recompression static pressure distribution is a function of the combined inviscid flow field and the mixing zone flow field. The following discussion treats the theoretical inviscid flow field and the superposition of a mixing zone.

### 2.1 THEORETICAL INVISCID JET FLOW FIELD

A typical axisymmetric ejector system is shown in Fig. 1. The inviscid flow field of the jet emanating from the nozzle exit can be determined by applying the method of characteristics solution to the

general potential flow field equations using the known nozzle exit flow conditions and the cell pressure ratio  $\left(\frac{p_c}{p_t}\right)$ . This method is adequately covered in Ref. 10 for both isentropic (irrotational) and rotational (total pressure gradient) flow. From the practical point of view, the assumption of isentropic flow simplifies the flow field calculation; however, this obviously is a questionable assumption if the nozzle exit flow is known to be highly rotational because of the contour of the nozzle. Even if the nozzle flow is isentropic, the jet flow field cannot be treated in general as isentropic flow because of the presence of a shock wave referred to herein as the jet boundary shock wave. The jet boundary shock wave is formed by the coalescence of infinitesimal compression waves which result from the curvature of the axisymmetric constant pressure jet boundary (Ref. 11). The strength (change in entropy) of the jet boundary shock wave increases with jet radius. Fortunately, for most ejector systems, the jet impinges on the diffuser wall before the boundary shock wave can develop significant strength and therefore may be treated as isentropic. This is also indicated by the fact that the location of the inviscid jet boundary can be accurately calculated neglecting the boundary shock wave.

## 2.2 EXPERIMENTAL VERIFICATION OF THEORETICAL INVISCID FLOW FIELD

On the basis of the previous discussion the jet flow field is assumed to be isentropic and is theoretically treated by the method presented in Ref. 12. To verify this theoretical method, lines of constant Mach number in the free jets of two ejector systems were experimentally determined from total pressure measurements and the assumption of isentropic flow. Thus, the total pressure anywhere in the flow field was assumed to be equal to the nozzle plenum total pressure. Since a total pressure probe in a supersonic stream measures the total pressure downstream of a normal shock wave, the ratio of measured total pressure to nozzle plenum total pressure can be used to determine the free-stream Mach number.

The two ejector systems tested used 18-deg, half-angle conical driving nozzles having area ratios of 10.848 and 25.000, which are described in Ref. 4. The diffuser diameter for both configurations was 10.19 in. The total pressures in the internal portion of the jet flow field were measured by a fixed rake (Fig. 2a), and the driving nozzle was axially translatable relative to the fixed rake; thus measurements could be obtained at various axial stations. A complete description of the rake and movable nozzle system is presented in Ref. 6. The driving fluid was unheated air at a temperature of about 80°F.



The theoretical flow field, based on the assumption of isentropic flow, is shown in Figs. 3 and 4 to agree well with the experimental results for the internal portion of the free jet. The theoretical flow field was calculated by the IBM 7070 computer. The experimental results presented in Figs. 3 and 4 were obtained by cross-plotting the original experimental data in such a manner as to obtain lines of constant Mach number.

Experimental flow field measurements in the vicinity of the jet boundary were made with a single total pressure probe, approximately aligned with the flow direction as shown in Fig. 2b. The jet flow field in this region cannot be assumed to be irrotational (constant total pressure) because of the mixing zone and the jet boundary shock wave. Therefore, the measured total pressure cannot be used to determine Mach number without making further assumptions concerning the nature of the actual flow field or by measuring the static pressures. Static pressure measurements in this portion of the flow field are impracticable by conventional methods because of the non-uniformity of the flow field. To avoid these difficulties, the ratio of the experimentally measured total pressure to the nozzle total pressure is compared in Fig. 5 with the theoretical total pressure that the probe should sense. This comparison shows that the theoretical location of the jet boundary shock wave and the flow conditions upstream of the boundary shock wave agree well with the experimental results. It is also shown in Fig. 5 that in the region between the jet boundary shock wave and the inviscid jet boundary, the theoretical flow field is in error because of the previously mentioned presence of the mixing zone and the nonisentropic nature of the jet boundary shock wave. For the particular ejector systems used in these experiments, the theoretical maximum total pressure loss through the jet boundary shock wave is less than 5 percent. Therefore, the mixing zone is the primary cause of the disagreement between the theory and experiment in this region for these particular configurations.

In summary, it can be concluded that the jet flow field, out to the impingement shock wave, is accurately predicted by applying the method of characteristics solution to the general isentropic flow equations except in the region of the mixing zone.

### 2.3 THEORETICAL RECOMPRESSION STATIC PRESSURE DISTRIBUTION

The flow field approaching the diffuser wall is rotational in the mixing zone portion and non-uniform in the inviscid portion. The turning of such a flow field parallel to a wall can be treated theoretically (neglecting boundary layer) to determine the static pressure distribution

along the wall by considering small increments in the approaching flow to be uniform at some average Mach number, flow direction, and total pressure level. The impingement shock wave can be treated as two-dimensional for most systems of practical interest since it is always at a large radius from the centerline of the nozzle. A sketch of a representative first-order theoretical recompression flow field is presented in Fig. 6. This is referred to as a first-order theory since the weaker or second-order interaction waves are neglected. The calculation procedure involves the following:

1. The pressure  $p_{11}$  is produced by the turning (two-dimensionally of the average flow conditions in region 1 through the angle  $\left[\frac{\beta + \beta_1}{2}\right]$ .
2. The average flow in region 2 turns through the angle  $\left[\left(\frac{\beta_1 + \beta_2}{2}\right) - \delta_1\right]$  in order to satisfy the interaction conditions with the downstream flow from region 1. The interaction conditions are: equal static pressures ( $p_{21} = p_{22}$ ) and parallel flow. Thus, the angle  $\delta_1$  can be determined by a trial and error procedure. The magnitude of the angle  $\delta_1$  is typically about 1 deg or less, depending on the size of the region. Therefore, the pressure  $p_{21}$  is determined by an isentropic compression from  $p_{11}$  through the angle  $\delta_1$ .
3. The pressure  $p_{31}$  is produced by an isentropic compression from  $p_{21}$  through the angle  $\delta_1$ . The pressure  $p_{32}$  is produced by an isentropic compression from  $p_{22}$  through the angle  $\delta_1$ . When second-order compression and expansion waves are neglected,  $p_{32} = p_{31}$ .
4. The pressure  $p_{41}$  is produced by an isentropic compression from  $p_{31}$  through the angle  $\delta_2$ . The pressure  $p_{42}$  is produced by an isentropic compression from  $p_{32}$  through the angle  $\delta_2$ . The pressure  $p_{43}$  is produced by the turning of the average flow in region 3 through the angle  $\delta_2$  in such a manner as to satisfy the previously stated interaction conditions. When second-order waves are neglected,  $p_{43} = p_{42} = p_{41}$ .
5. The pressure  $p_{51}$  is produced by an isentropic compression from  $p_{41}$  through the angle  $\delta_2$ . The pressure  $p_{52}$  is produced by an isentropic compression from  $p_{42}$  through the angle  $\delta_2$ . The pressure  $p_{53}$  is produced by isentropic compression from  $p_{43}$  through the angle  $\delta_2$ . When second-order waves are neglected,  $p_{51} = p_{52} = p_{53}$ .

Steps 1 through 5 treat the theoretical recompression of the mixing zone portion of the approaching flow field. The theory shows that the static pressure distribution along the diffuser wall is of an increasing nature from  $p_{11}$  to  $p_{s,1}$  - produced by a series of isentropic compressions. It is also shown that the approaching flow does not turn parallel to the diffuser wall, initially, but through the angle  $(\beta - \delta)$ . The flow is then turned parallel to the diffuser wall by an isentropic compression through the angle  $\delta$ .

The theoretical recompression of the inviscid portion of the approaching flow (constant total pressure and increasing Mach number) can be treated in a similar manner.

6. The pressure  $p_{s,4}$  is produced by the turning of the average flow conditions in region 4 through the angle  $\left[ \frac{\beta_3 + \beta_4}{2} + \delta_3 \right]$  in such a manner as to satisfy the interaction conditions with the downstream flow from region 3.

The interaction conditions require the downstream flow from region 3 to expand isentropically through the angle  $\delta_3$  to the pressure  $p_{s,3}$  because of the characteristics of the two-dimensional shock wave theory shown, for a typical case, in Fig. 7 (decreasing downstream static pressure with Mach number). Therefore, the pressure  $p_{s,2}$  is produced by an isentropic expansion from  $p_{s,2}$  through the angle  $\delta_3$ . The pressure  $p_{s,1}$  is produced by an isentropic expansion from  $p_{s,1}$  through the angle  $\delta_3$ . When second-order waves are neglected,  $p_{s,4} = p_{s,3} = p_{s,2} = p_{s,1}$ .

7. The pressure  $p_{7,1}$  is produced by an isentropic expansion from  $p_{s,1}$  through the angle  $\delta_3$ . In a similar manner the pressures  $p_{7,2}$ ,  $p_{7,3}$ , and  $p_{7,4}$  are determined. When second-order waves are neglected,  $p_{7,4} = p_{7,3} = p_{7,2} = p_{7,1}$ .
8. The above procedure is repeated for regions 5, 6, 7, etc.

Steps 6 through 8 show the theoretical diffuser wall static pressure distribution to be of a decreasing nature from  $p_{s,1}$ . This analysis also shows that the approaching flow does not turn parallel to the diffuser wall, initially, but through the angle  $(\beta + \delta)$ . The flow is then turned parallel to the diffuser wall by an isentropic expansion through the angle  $\delta$ .

The error in this theory caused by neglecting the second-order waves can be estimated in the following manner. The flow interaction requirements which determine the impingement shock wave are equal static pressures and flow direction. However, the Mach numbers in the two regions produced by the interaction will be different because



of the differences in the total pressure levels. As an example, the Mach number in the region where  $p_{21}$  exists may be 1.60 and the Mach number in the region where  $p_{22}$  exists may be 2.6, depending on the size of the flow field increment. If  $\delta_1 = 1.0$  deg, then from Fig. 8 for an isentropic compression,

$$\frac{p_{31}}{p_{21}} = 1.051$$

and

$$\frac{p_{32}}{p_{22}} = 1.071$$

Since  $p_{21} = p_{22}$ , second-order waves are necessary to satisfy the interaction conditions. Neglecting second-order waves results in an error of +1.91 percent in  $p_{32}$  relative to  $p_{31}$ . The difference in Mach number used in this example is relatively large; a typical Mach number difference would be 0.25, and the corresponding error in  $p_{32}$  relative to  $p_{31}$  would be 0.42 percent. The curves in Fig. 8 show the relative insensitivity of the pressure ratio with Mach number for Mach numbers greater than 1.1. Thus, the first-order theoretical recompression analysis is accurate for at least that portion of the recompression static pressure distribution from the stagnating streamline to a point slightly beyond the peak static pressure location.

For typical flows considered, the theoretical peak recompression static pressure is  $p_{s,1}$  and is shown in step 5 to be equal to  $p_{s,3}$ . The pressure  $p_{s,3}$  is determined by the average flow conditions in the vicinity of the inner edge of the mixing zone (region 3). Since the initial turning angle of the mixing zone portion of the approaching flow field is  $(\beta - \delta)$  and since the initial turning angle of the inviscid portion of the approaching flow field is  $(\beta + \delta)$ , then the streamline along the inner edge of the mixing zone must turn through the angle  $\beta$ . Thus, the end of the compression process and beginning of the expansion process is determined by the location of the inner edge of the mixing zone. As a result, the peak recompression static pressure is equal to the static pressure downstream of the impingement shock wave required to turn the flow along the inner edge of the mixing zone parallel to the diffuser wall.

## 2.4 SIMPLIFIED THEORETICAL RECOMPRESSION STATIC PRESSURE DISTRIBUTION

The first-order theoretical recompression static pressure distribution involves a trial and error procedure to determine  $\delta$  and a scale drawing of the flow field to determine the shock wave arrangement. The recompression static pressure distribution can be approximated by ignoring the actual impingement shock wave configuration and the flow field interactions. The procedure is to determine the flow conditions approaching the diffuser wall at each point and to turn each streamline parallel to

the wall through an oblique shock. Two types of error exist in this simplified analysis. One error is associated with the orientation of the flow and the other is associated with the magnitude of the static pressure. The orientation error is not significant if the angle, relative to the diffuser wall, of the approaching flow field is approximately equal to the Mach angle of the flow downstream of the impingement shock wave. This is usually the case for many ejector systems. The error in the magnitude of the static pressure can be estimated in the following manner. Consider the streamline approaching the diffuser wall that has the same flow conditions as the average flow in region 2 (Fig. 6). Let  $p_3$  be the static pressure downstream of the two-dimensional shock wave required to bend this streamline parallel to the wall. The turning angle would be  $\left(\frac{\beta_1 + \beta_2}{2}\right)$ . The static pressure  $p_3$  can be approximated by considering that this streamline turns by means of a two-dimensional shock wave through the angle  $\left[\frac{\beta_1 + \beta_2}{2} - \delta_1\right]$  and then isentropically compresses through the angle  $\delta_1$  to the static pressure  $p'_3$ . The error in  $p'_3$  relative to  $p_3$  for  $\delta_1 = 1$  deg is shown to be very small in Fig. 9 for typical flow conditions. In steps 2 and 3 (section 2.3) the static pressure  $p_{32}$  is shown to be determined by the same process as that used to determine  $p'_3$ . Therefore,  $p_3 = p'_3 = p_{32} = p_{31}$ . Thus, the error in the magnitude of the static pressure obtained by this simplified analysis is on the order of that produced by neglecting second-order waves (section 2.3).

## 2.5 SUPERPOSITION OF MIXING ZONE ON INVISCID FLOW FIELD

The theoretical recompression of a known approaching flow field is presented in sections 2.3 and 2.4. However, for axisymmetric jets, the mixing takes place in a region of non-uniform flow both along and across the mixing zone. The greatest flow field variation is in the direction across the mixing zone, as shown in Figs. 10a and 11a. These flow conditions violate the basic assumptions of uniform flow and constant static pressure made in Ref. 7 to theoretically determine the velocity distribution in the mixing zone. Therefore, a direct superposition of this theoretical mixing zone velocity profile on the theoretical inviscid flow field of an axisymmetric jet is unjustifiable. However, as previously stated in this report, only the peak recompression static pressure is of importance in Korst's supersonic base pressure theory. In section 2.3 it is theoretically shown that the peak recompression static pressure is produced by the turning, parallel to the diffuser wall, of the flow field along the inner edge of the mixing zone.

A comparison of experimental recompression static pressure distribution with the simplified theoretical distribution based on the

isentropic inviscid flow field is presented in Figs. 10b and 11b. The theoretical distribution is shown to be in error due to neglecting the mixing process. However, the theoretical distribution is shown to agree reasonably well with the experimental data in the region downstream of the apparent mixing zone, thus verifying the simplified theoretical analysis.

The region of maximum influence of the mixing process relative to the inviscid flow field can be estimated from an idealized conception of the recompression flow phenomena. Based on the results presented in Figs. 10b and 11b, an idealized recompression flow model was developed as shown in Figs. 12a and b. The region of influence of the mixing zone on the recompression static pressure distribution can be determined in the following manner:

a. Impingement location of the inner edge of the mixing zone

$$\frac{\Delta x_3}{r_{ne}} = \frac{k}{\sin \beta} \left( \frac{b}{r_{ne}} \right) \quad (1)$$

For turbulent mixing

$$\frac{b}{r_{ne}} = c \left( \frac{l_j}{r_{ne}} \right) \quad (2)$$

Substituting Eq. (2) into Eq. (1) yields

$$\frac{\Delta x_3}{r_{ne}} = \frac{k c}{\sin \beta} \left( \frac{l_j}{r_{ne}} \right) \quad (3)$$

Values for  $k$  and  $c$  (from Abramovich, Ref. 13) are derived in Ref. 9 and presented in Fig. 13. Values for  $\frac{l_j}{r_{ne}}$  and  $\beta$  are obtained from the theoretical inviscid jet boundary.

b. Impingement location of stagnating streamline

The thickness of the mixing zone at the impingement point of the stagnating streamline is

$$\frac{b}{r_{ne}} = c \left[ \frac{l_j}{r_{ne}} - \frac{\Delta x_2}{r_{ne}} \cos \beta \right] \quad (4)$$

by geometry

$$\frac{\Delta x_2}{r_{ne}} = \frac{\left( \frac{b}{r_{ne}} \right)}{\sin \beta} \left( \frac{\eta_\infty - \eta_s}{2\eta_M} \right) \quad (5)$$

by definition (Ref. 9)

$$k = \frac{\eta_M - \eta_\infty}{2\eta_M} \quad (6)$$

Substituting Eqs. (4) and (6) into Eq. (5) and solving for  $\frac{\Delta x_2}{r_{ne}}$  yields

$$\frac{\Delta x_2}{r_{ne}} = \frac{k c \left( \frac{l_j}{r_{ne}} \right) \left( \frac{\eta_\infty - \eta_s}{\eta_M - \eta_\infty} \right)}{\sin \beta \left[ 1 + \frac{k c}{\tan \beta} \left( \frac{\eta_\infty - \eta_s}{\eta_M - \eta_\infty} \right) \right]} \quad (7)$$

c. Location of outer edge of mixing zone

The equation for the thickness of the mixing zone is

$$\frac{b}{r_{ne}} = c \left[ \frac{l_j}{r_{ne}} - \left( \frac{\Delta x_2}{r_{ne}} \right) \cos \beta - \frac{\Delta x_1}{r_{ne}} \right] \quad (8)$$

By geometry,  $\frac{\Delta x_1}{r_{ne}}$  can be approximated by the following equation

$$\frac{\Delta x_1}{r_{ne}} = \left[ (1 - k) \left( \frac{b}{r_{ne}} \right) - \left( \frac{\Delta x_2}{r_{ne}} \right) \sin \beta \right] \left( \frac{1}{\tan \frac{\beta}{2}} \right) \quad (9)$$

Substituting Eq. (8) into Eq. (9) and solving for  $\frac{\Delta x_1}{r_{ne}}$  yields

$$\frac{\Delta x_1}{r_{ne}} = \frac{(1 - k) c \left( \frac{l_j}{r_{ne}} \right) - [(1 - k) c + \tan \beta] \left( \frac{\Delta x_2}{r_{ne}} \right) \cos \beta}{\left[ (1 - k) c + \tan \frac{\beta}{2} \right]} \quad (10)$$

The location  $\eta_s$  of the stagnating streamline is determined by the condition that the total pressure of the stagnating streamline equals the peak recompression static pressure.

The theoretical mixing zone width determined by Eqs. (3), (7), and (10) is shown in Figs. 10b and 11b to agree very well with the apparent experimental width of the mixing zone. It is also shown in Figs. 10b and 11b that the theoretical recompression static pressure determined by the inviscid flow conditions along the inner edge of the mixing zone agrees in magnitude with the experimental peak recompression static pressure.

## 2.6 EXPERIMENTAL VERIFICATION OF THE THEORETICAL PEAK RECOMPRESSION STATIC PRESSURE

In section 2.3, it was theoretically shown that the peak recompression static pressure is determined by turning, parallel to the diffuser wall, the inviscid flow along the inner edge of the mixing zone. Theoretical peak recompression static pressures are compared with experimental values in Figs. 14 and 15. The theoretical values were obtained



by using the method of characteristics solution to the general potential isentropic flow equations to determine the inviscid flow field, based on the experimental  $\left(\frac{p_c}{p_t}\right)$  and Eq. (3) to determine the location of the inner edge of the mixing zone. The experimental data were obtained from three ejector systems geometrically described in each figure. The minimum cell pressure ratio  $\left(\frac{p_c}{p_t}\right)$  for each configuration was varied by varying the total pressure ( $p_t$ ) level of the driving nozzle. The resulting variation of  $(p_c/p_t)$  with  $p_t$  is shown in Fig. 16 and is due to a Reynolds number effect described in Ref. 4. The Reynolds number determines the character of the nozzle boundary layer which then influences the free-jet mixing process, thus producing a new equilibrium cell pressure. The nozzle boundary layer influences the jet mixing process in two ways.

1. The velocity profile in the mixing zone varies in shape with distance from the nozzle exit. However, the asymptotic profile is the same as the undisturbed mixing profile.
2. The mixing zone has a finite thickness at the nozzle exit and, consequently, is thicker, at any point, than the undisturbed mixing zone.

Theoretically, the two characteristics of the mixing zone, which are involved with the peak recompression static pressure, are  $k$  and  $b$ . The relative location ( $k$ ) is a function of the velocity profile in the mixing zone. The width ( $b$ ) of the mixing zone at the point of impingement is a function of the thickness of the mixing zone at the nozzle exit. For most ejector systems of practical interest, the length of the mixing zone is sufficient to allow the velocity profile to transform into the undisturbed profile. Thus, the relative location ( $k$ ) is the same as for the undisturbed case. However, the width of the mixing zone ( $b$ ) for most ejector systems of practical interest will be thicker than the undisturbed case and will produce a lower peak recompression static pressure than the undisturbed case. This is experimentally verified in Figs. 15b and c by comparing the theoretical peak recompression static pressure for an undisturbed mixing zone with the experimental values obtained at low total pressure levels (low Reynolds number). The comparison in Fig. 15 shows that the theoretical peak recompression static pressure determined by the flow conditions along the inner edge of the mixing zone agrees to within 10 percent of the experimental values of the maximum total pressure level. Included in Figs. 14 and 15 is the peak recompression static pressure that would exist if there were no mixing. This is the recompression static pressure produced by the turning of the inviscid jet boundary streamline parallel to the diffuser wall.

Since the major factor which determines the peak recompression static pressure is  $(P_c/P_t)$ , theoretical peak recompression static pressures are compared with experimental values in Fig. 14 as a function of  $(P_c/P_t)$ . These are the same experimental values as presented in Fig. 15. Included in Fig. 14c are experimental peak recompression static pressures obtained with a small amount of bleed flow into the cell region. The bleed flow caused the cell pressure ratio to increase to a new equilibrium value and a new peak recompression static pressure. The theoretical peak recompression static pressures determined by the flow conditions along the inner edge of the mixing zone are shown in Fig. 14c to agree very well with the new experimental values. Further experimental verification of the recompression theory is presented in Table 1, in which the theory is compared with data obtained from Ref. 8.

From the previous discussion it can be concluded that the peak recompression static pressure determined by the flow conditions along the inner edge of the mixing zone agrees with the experimental results to within  $\pm 10$  percent for those cases in which the nozzle exit boundary layer can be neglected.

### 3.0 THEORETICAL MINIMUM CELL PRESSURE RATIO OF AXISYMMETRIC EJECTOR SYSTEMS

Korst (Ref. 7) has developed the two-dimensional, supersonic base pressure theory for negligible initial boundary layer. When trying to apply this theory to an axisymmetric ejector system, most of the basic assumptions (discussed in Ref. 8) are clearly violated. Also in Refs. 8 and 9 it is shown that the total pressure on the dividing streamline is, for most practical ejector systems, independent of axisymmetric effects. The non-uniformity of the inviscid flow would be expected to produce a significant deviation from the two-dimensional value of the total pressure on the dividing streamline; however, in Ref. 8 and indirectly by the data in this report no appreciable deviation was noted. A possible explanation of this is the following. The non-uniformity of the inviscid flow field distorts the mixing zone in such a manner as to cause the total pressure on the dividing streamline to be greater than the two-dimensional value (Ref. 8). The dividing streamline may then experience a normal shock before stagnating on the diffuser wall (Ref. 17), thus reducing the total pressure. These two processes tend to cancel each other, resulting in a total pressure level close to the two-dimensional isentropic recompression pressure.

As previously stated, the major source of error associated with the application of the two-dimensional base pressure theory to an axisymmetric ejector system is the assumption of uniform inviscid flow in the determination of the peak static pressure in the impingement zone. This error in Korst's base pressure theory has been eliminated by using the recompression theory developed herein. The resulting base pressure theory is referred to as the "modified" base pressure theory.

A comparison of theoretical minimum cell pressure ratios with experimental data is presented in Fig. 16 for various axisymmetric ejector systems. The theoretical values were obtained by using the base pressure theory (isoenergetic, neglecting initial boundary layer) presented in Ref. 7 modified by the theory developed in this report for estimating the peak recompression static pressure. Included in Figs. 16a and b are theoretical minimum cell pressure ratios using the unmodified two-dimensional theory. As shown in Figs. 16a through e, the modified theory agrees very well with experimental results, except for the two ejector configurations in Figs. 16d and e which were using "bell" type nozzles. Theoretically, these two ejector configurations were treated as having isentropic nozzles with uniform exit flow conditions; this, of course, is not correct since the total pressure and velocity vary non-uniformly across the exit. This is believed to be the reason for the major portion of the difference between the theoretical and experimental values obtained for these two configurations.

All of the data presented in Fig. 16 were obtained from ejector systems using air ( $\gamma = 1.4$ ) as the driving fluid and having nozzle exit flow angles of 0, 15, and 18 deg. In Table 2 theoretical minimum cell pressure ratios are compared with experimental values (Ref. 14) for an ejector system using a conical nozzle having a half angle of 7.58 deg. This system was operated using both air ( $\gamma = 1.40$ ) and helium ( $\gamma = 1.66$ ) as the driving fluids; the theoretical minimum cell pressure ratios are shown to agree very well with the experimental values.

In summary, the theoretical results were compared with experimental values obtained from 34 axisymmetric ejector systems, neglecting "bell" ejector systems, having the following characteristics:

$$\begin{aligned} \gamma &= 1.4 \quad \text{and} \quad 1.66 \\ 1.00 &\leq \frac{A_{ne}}{A^*} \leq 25.00 \\ 1.46 &\leq \frac{A_D}{A^*} \leq 150.36 \\ 0 \text{ deg} &\leq \theta_{ne} \leq 18 \text{ deg} \end{aligned}$$

The use of the modified theory resulted in minimum cell pressure ratio values which deviated from the experimental values by a maximum of -11.8 to +25.2 percent, with a standard deviation of 5.5 percent (Ref. 15).

The modified base pressure theory also applies directly to the two-dimensional case with a curved jet boundary as compared with the simpler theory derived by Korst for straight jet boundaries. The modified base pressure theory shows, in general, that the minimum cell pressure ratio produced by an axisymmetric ejector system is a function of the thickness of the mixing zone at the free-jet boundary impingement point, unlike the two-dimensional back step case which has a uniform inviscid flow field.

#### 4.0 CONCLUSIONS

Based on the results of this study, the following conclusions are reached:

1. The peak recompression static pressure of an axisymmetric jet is approximately determined by the inviscid flow conditions along the inner edge of the mixing zone.
2. The peak recompression static pressure and therefore the minimum cell pressure ratio of an axisymmetric ejector system is, in general, a function of the thickness of the mixing zone at the free-jet boundary impingement point.
3. The minimum cell pressure ratio of the axisymmetric ejector systems investigated can be estimated to within 6 percent (standard deviation) through an application of Korst's isoenergetic, supersonic base pressure theory, modified by the recompression theory presented in this report. These results were verified for jet boundary Mach numbers from 1.6 to 7.4.



## REFERENCES

1. Barton, D. L. and Taylor, D. "An Investigation of Ejectors without Induced Flow - Phase I." AEDC-TN-59-145, December 1959.
2. Taylor, D., Barton, D. L., and Simmons, M. "An Investigation of Cylindrical Ejectors Equipped with Truncated Conical Inlets - Phase I." AEDC-TN-60-224, March 1961.
3. German, R. C. and Bauer, R. C. "Effects of Diffuser Length on the Performance of Ejectors without Induced Flow." AEDC-TN-61-89, August 1961.
4. Bauer, R. C. and German, R. C. "Some Reynolds Number Effects on the Performance of Ejectors without Induced Flow." AEDC-TN-61-87, August 1961.
5. Bauer, R. C. and German, R. C. "The Effect of Second Throat Geometry on the Performance of Ejectors without Induced Flow." AEDC-TN-61-133, November 1961.
6. German, R. C., Panesci, J. H., and Clark, H. K. "Zero Secondary Flow Ejector-Diffuser Performance Using Annular Nozzles." AEDC-TDR-62-196, January 1963.
7. Korst, H. H., Chow, W. L., and Zumwalt, G. W. "Research on Transonic and Supersonic Flow of a Real Fluid at Abrupt Increases in Cross Section." ME Technical Report 392-5, University of Illinois.
8. Zumwalt, G. W. "Analytical and Experimental Study of the Axially-Symmetric Supersonic Base Pressure Problem." Ph.D. Thesis, ME Dept., University of Illinois, 1959, MIC 59-4589, University Microfilms, Inc., Ann Arbor, Michigan.
9. Bauer, R. C. "Characteristics of Axisymmetric and Two Dimensional Isoenergetic Jet Mixing Zones." AEDC-TDR-63-253, December 1963.
10. Ferri, A. Elements of Aerodynamics of Supersonic Flows. The Macmillan Company, New York, 1949.
11. Lord, W. F. "On Axi-symmetrical Gas Jets, with Applications to Rocket Jet Flow Fields at High Altitudes." R & M No. 3235.

12. Moe, Mildred M. and Froesch, B. Andreas. "The Computation of Jet Flows with Shocks." STL-TR-0000-00661, May 1959.
13. Abramovich, G. N. "Turbulent Jets Theory." AD 283 858, August 3, 1962.
14. Hale, J. W. "Comparison of Diffuser-Ejector Performance with Five Different Driving Fluids." AEDC-TDR-63-207, October 1963.
15. Merriman, M. Method of Least Squares. John Wiley & Sons, Inc., New York, 1915.
16. Foster, R. M. "The Supersonic Diffuser and Its Application to Altitude Testing of Captive Rocket Engines." AFFTC-TR-60-1, January 1960.
17. Goethert, B. H. Base Flow Characteristics of Missiles with Cluster Rocket Exhausts." Aerospace Engineering, March 1961.

TABLE 1  
COMPARISON OF THEORETICAL WITH EXPERIMENTAL PEAK RECOMPRESSION STATIC PRESSURE

$\gamma = 1.4$

$\frac{A_{ne}}{A^*}$	$\frac{r_D}{r_{ne}}$	$\theta_{ne}$ deg	Nozzle Type	$\frac{p_c}{p_t}$	$\left(\frac{p_{wmax}}{p_c}\right)_{exp}$	$\left(\frac{p_{wmax}}{p_c}\right)_{theo}$	Error, percent	Remarks
1.0	2.00	0	Isentropic	0.05283	3.06	2.77	-9.48	Data from Ref. 8
1.1065	1.843	0	"	0.04149	3.18	3.56	+10.67	"
1.568	1.550	0	"	0.02274	3.68	4.05	+10.05	"
1.8562	1.440	0	"	0.01501	4.45	4.86	+9.21	"

TABLE 2  
 COMPARISON OF THEORETICAL WITH EXPERIMENTAL  
 MINIMUM CELL PRESSURE RATIOS OF AXISYMMETRIC EJECTORS

$\frac{A_D}{A^*}$	$\frac{A_{ne}}{A^*}$	$\theta_{ne}$ , deg	$\gamma$	$\left(\frac{P_c}{P_t}\right)_{exp}$	$\left(\frac{P_c}{P_t}\right)_{theo}$	Error, percent	Remarks
22.25	10.71	7.58	1.4	0.0011	0.000985	-10.46	Data from Ref. 14
22.25	10.71	7.58	1.66(He)	0.00068	0.000712	+4.71	
73.06	17.51	18	1.40	0.00045	0.00045026	+0.0578	

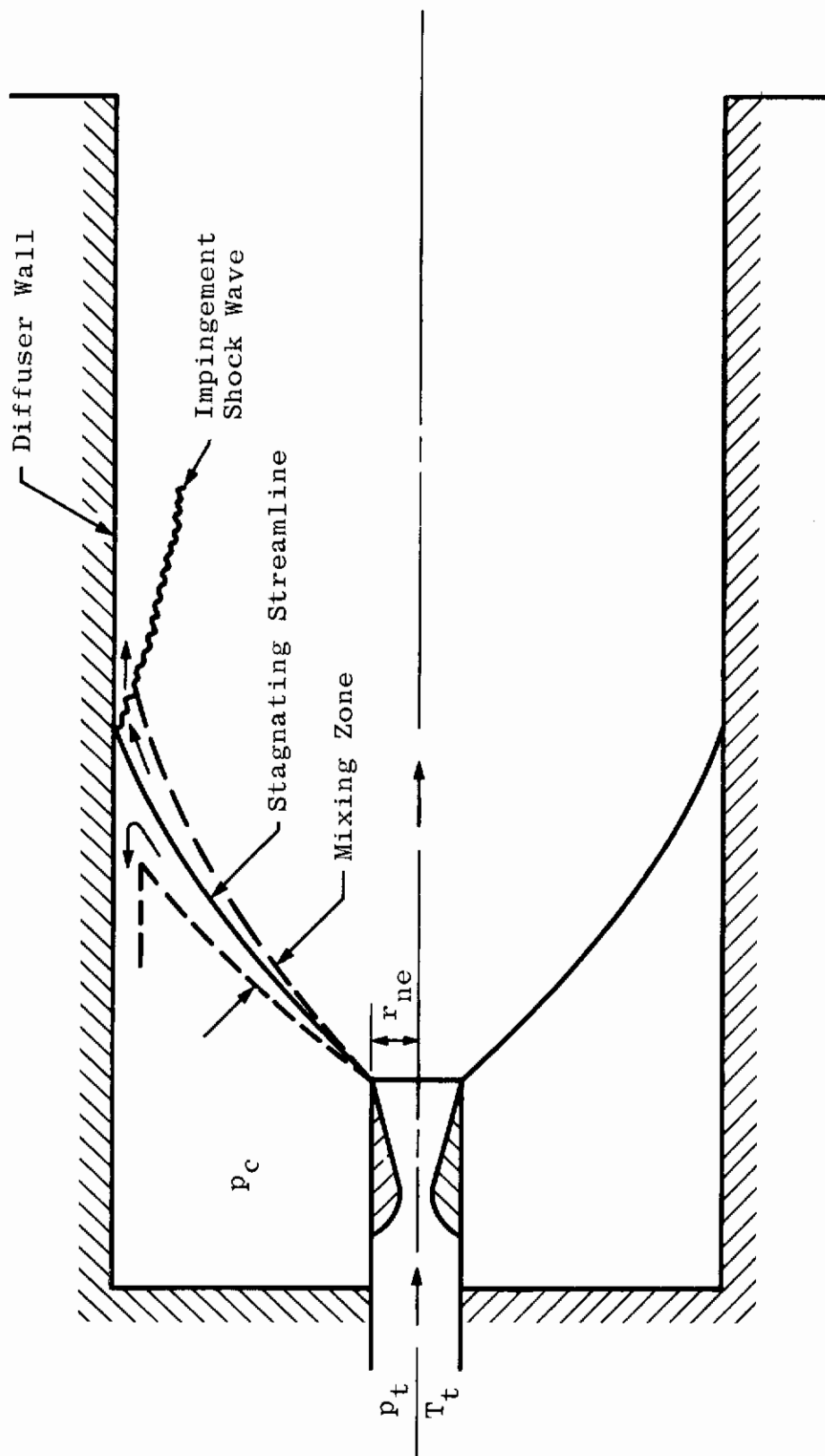
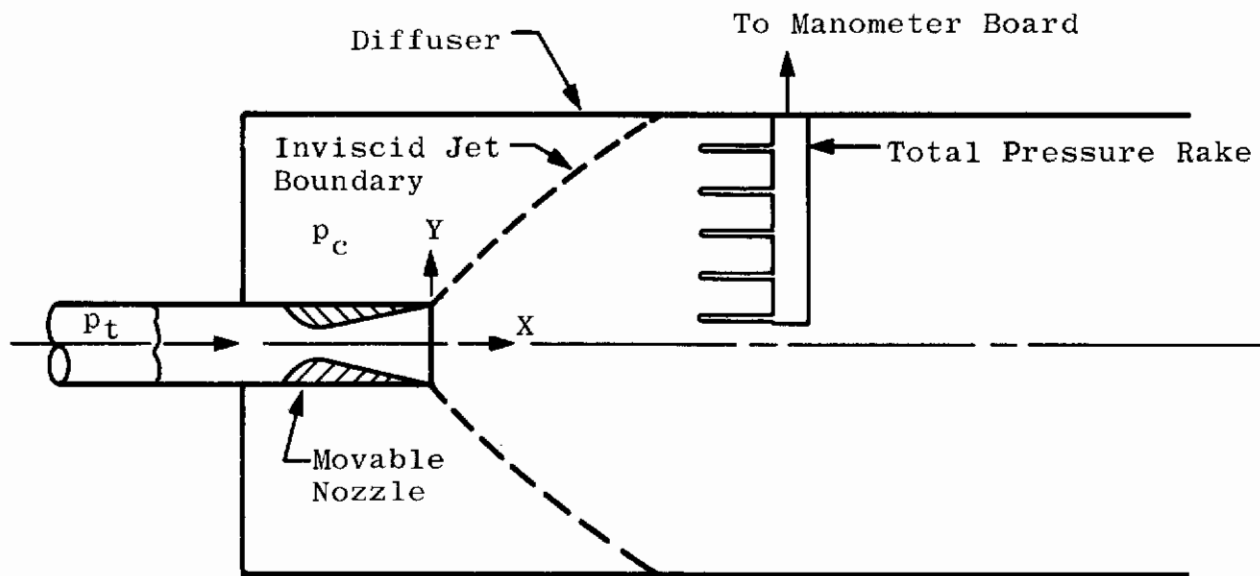
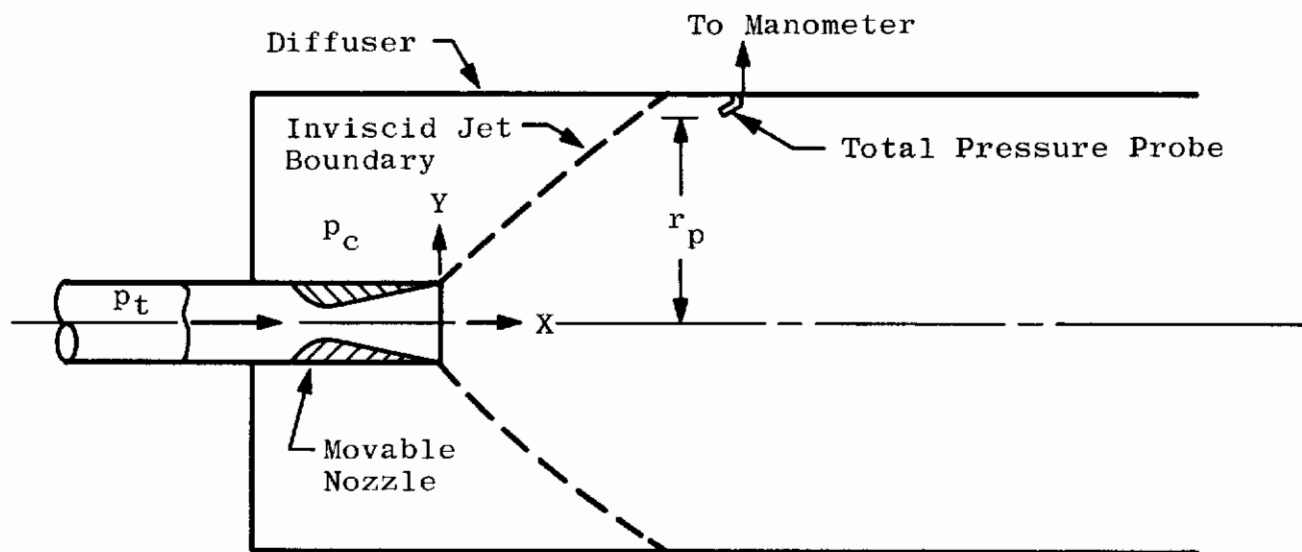


Fig. 1 Sketch of a Typical Ejector System



a. Total Pressure Rake Installation



b. Total Pressure Probe Installation

Fig. 2 Sketch of Experimental Configurations

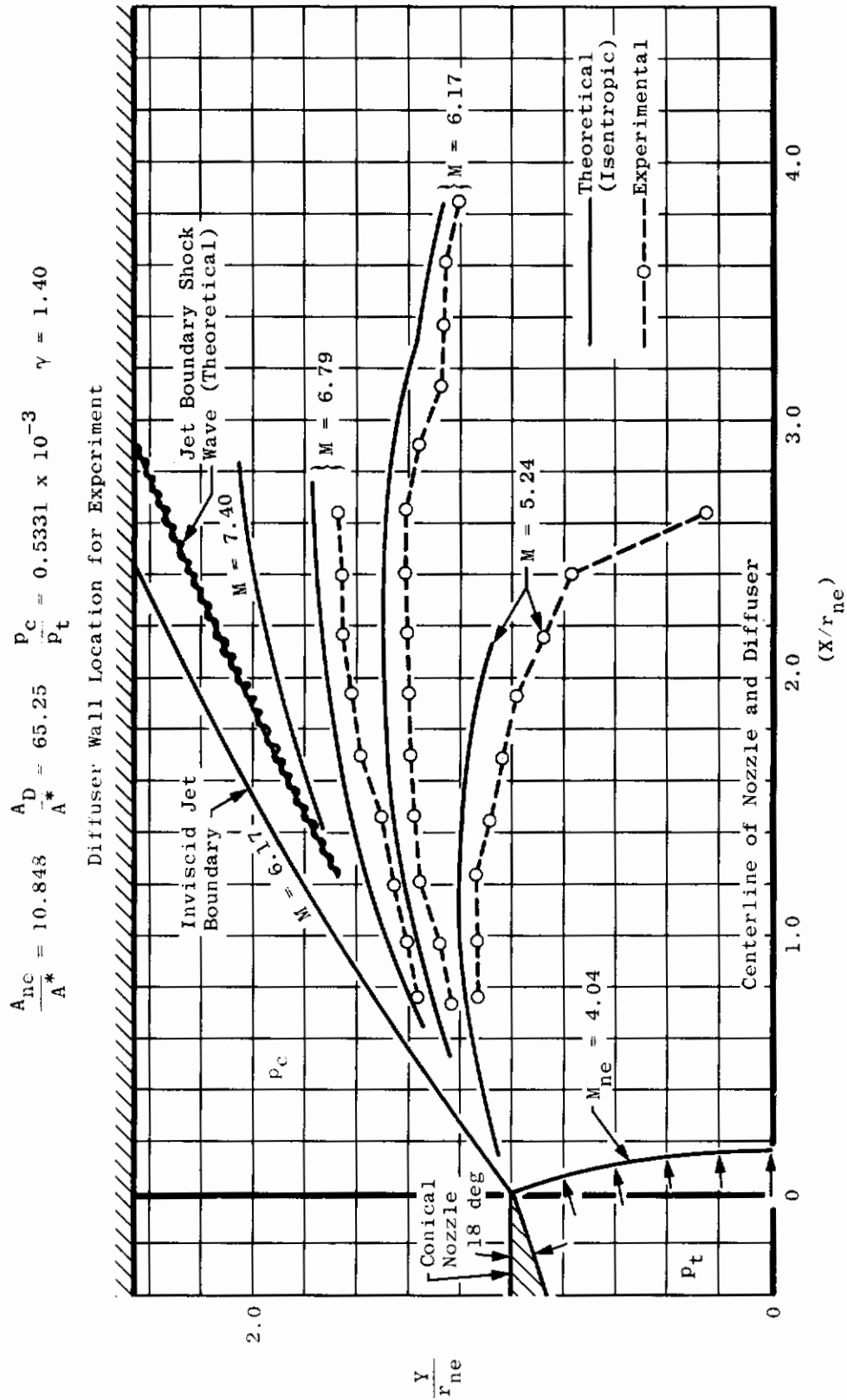


Fig. 3 Comparison of Theoretical with Experimental Lines of Constant Mach Number in a Free Jet,  $A_{ne}/A^* = 10.848$

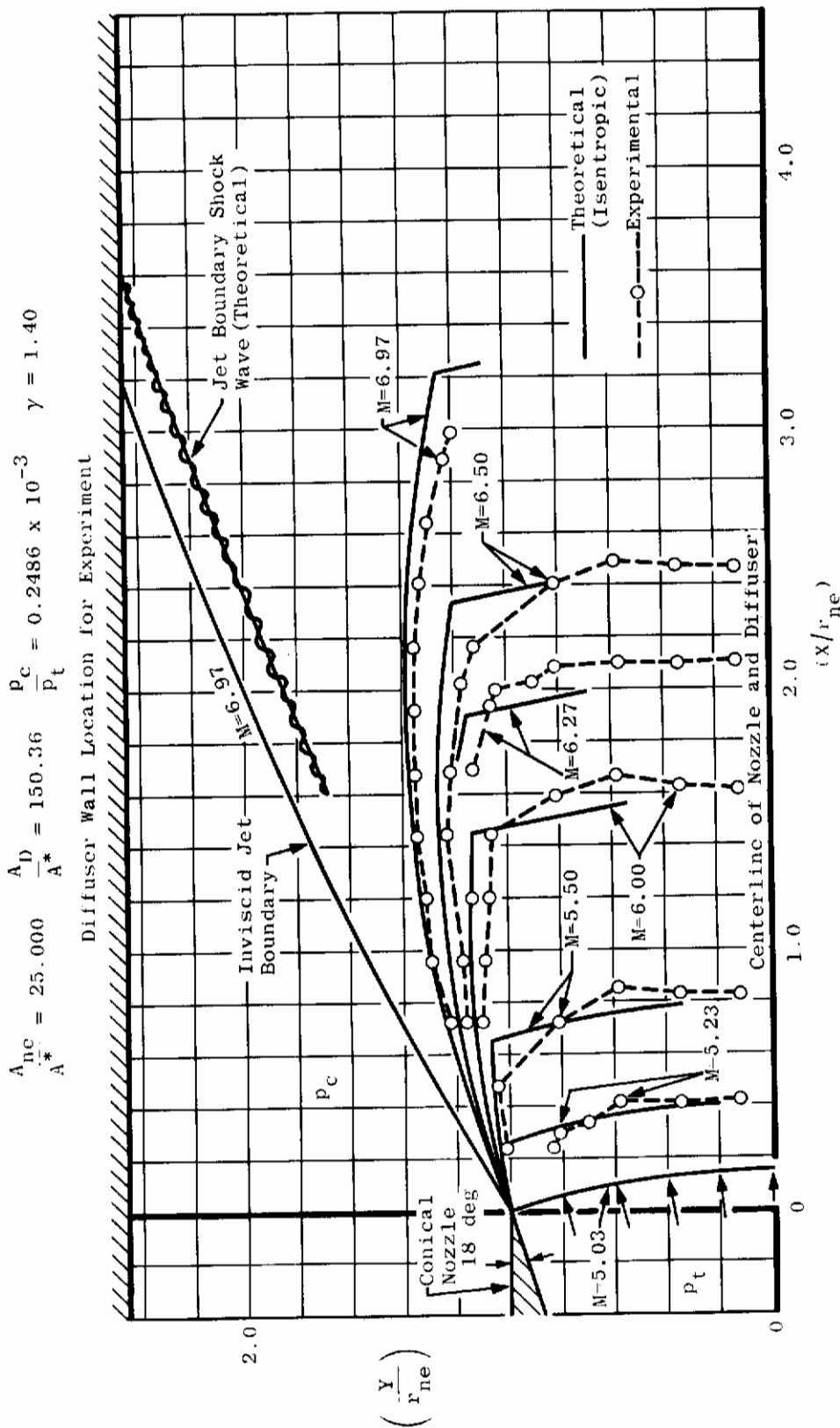
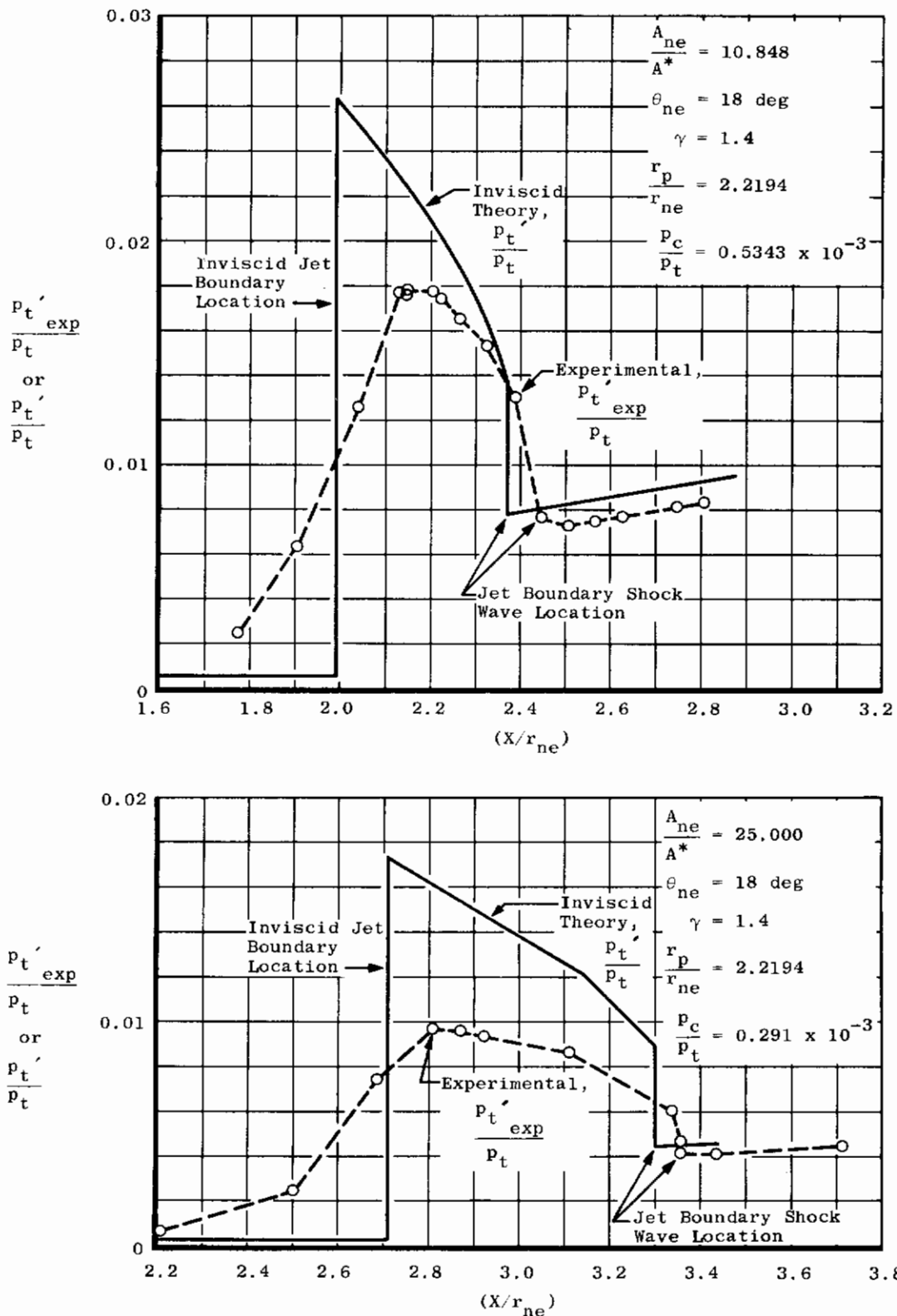


Fig. 4 Comparison of Theoretical with Experimental Lines of Constant Mach Number in a Free Jet,  $A_{ne}/A^* = 25.000$





**Fig. 5 Comparison of Theoretical with Experimental Measured Total Pressure in a Free Jet**

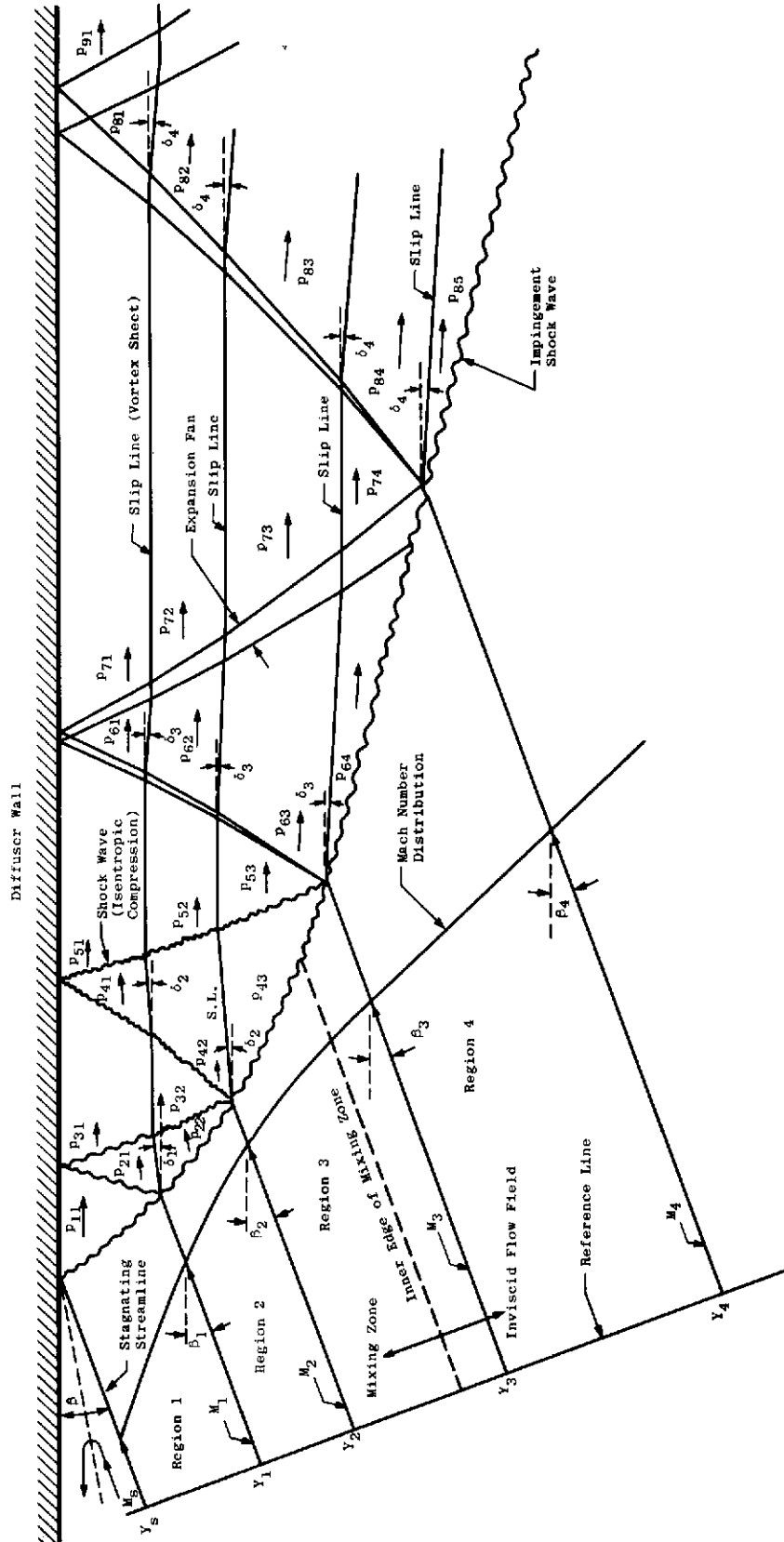


Fig. 6 Theoretical Recompression Flow Field (First Order)

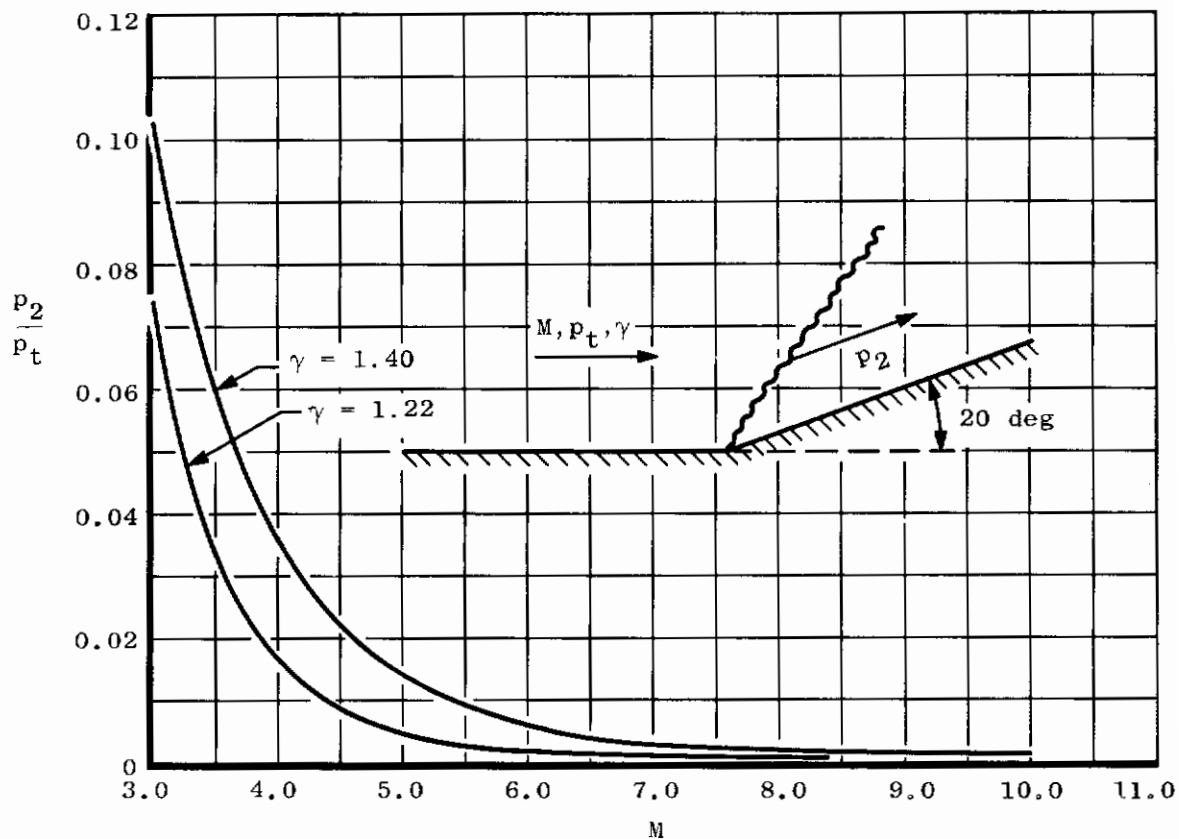


Fig. 7  $p_2/p_1$  vs  $M$  - Two-Dimensional Shock Wave Theory

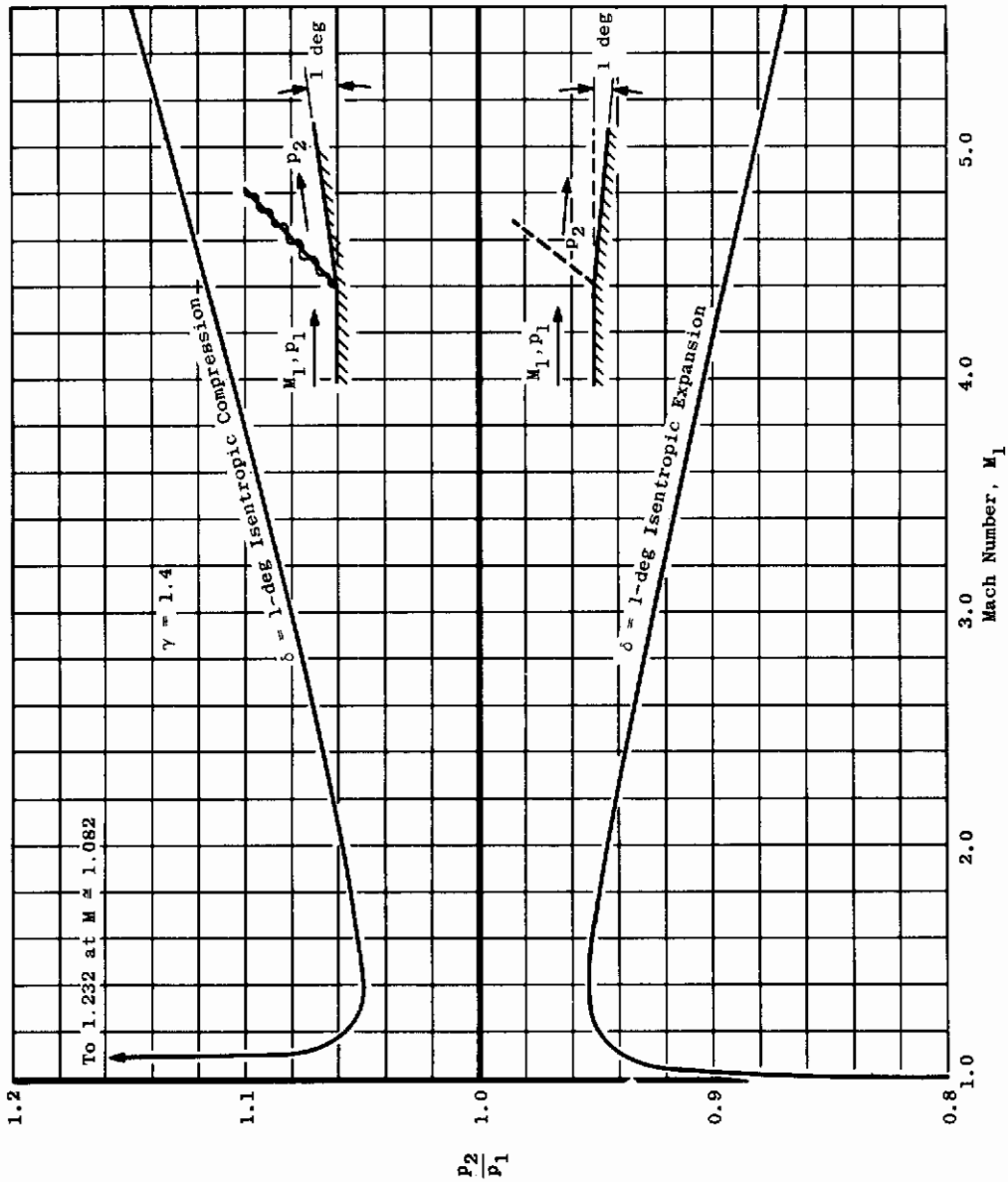


Fig. 8 Typical Isentropic Compression and Expansion Processes

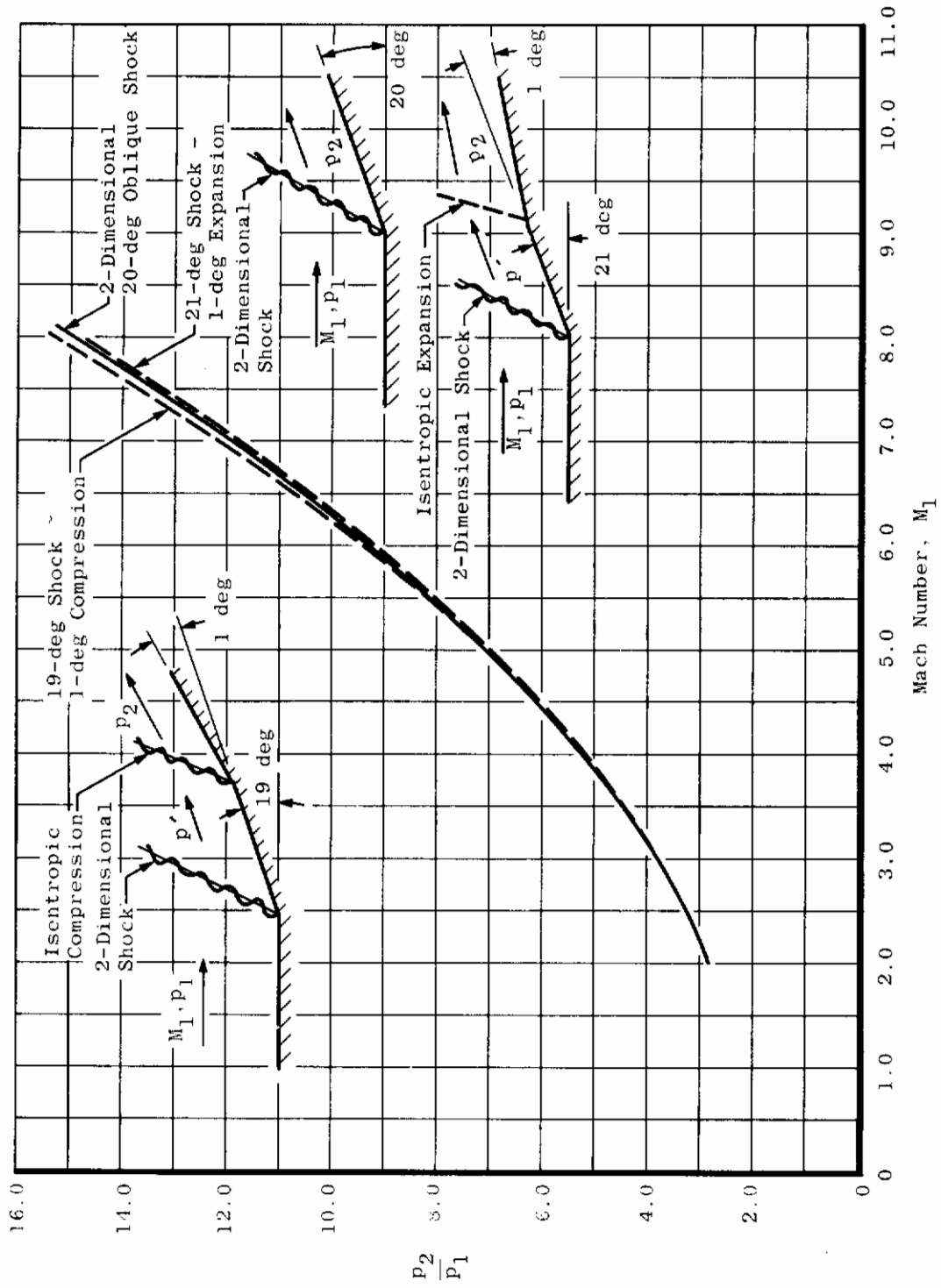
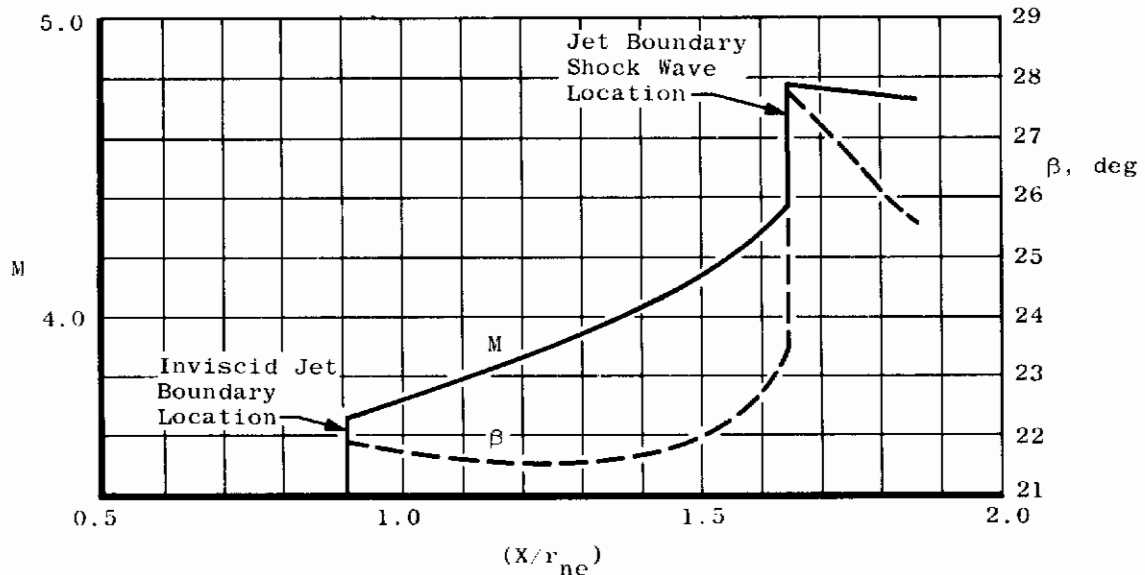
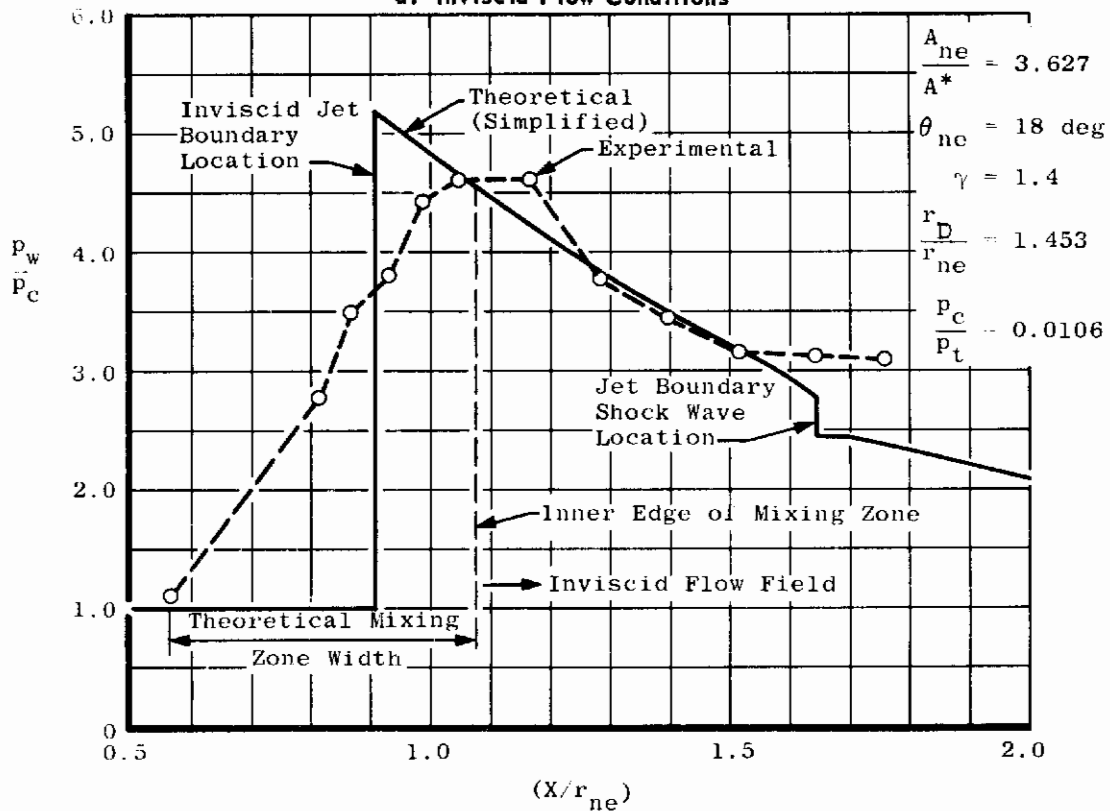


Fig. 9 Typical Error of Approximation to Two-Dimensional Shock Wave Theory

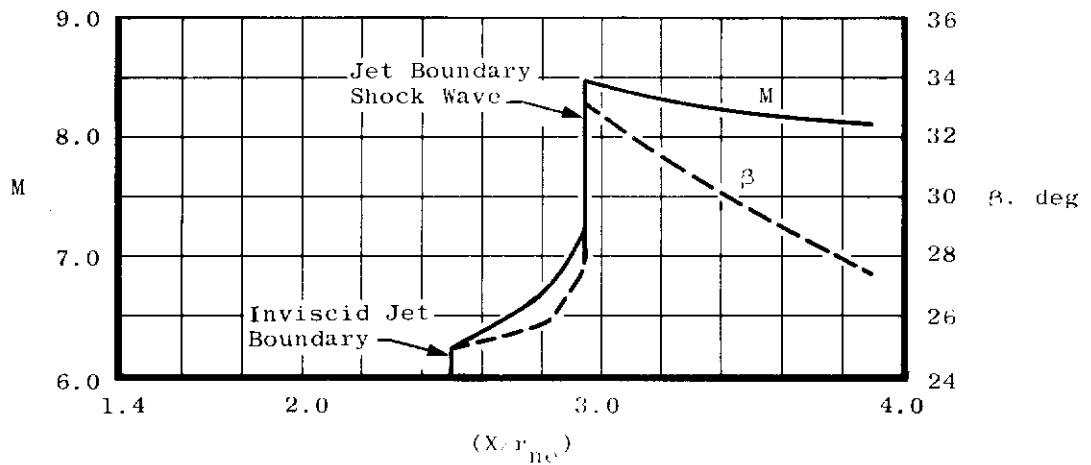


a. Inviscid Flow Conditions

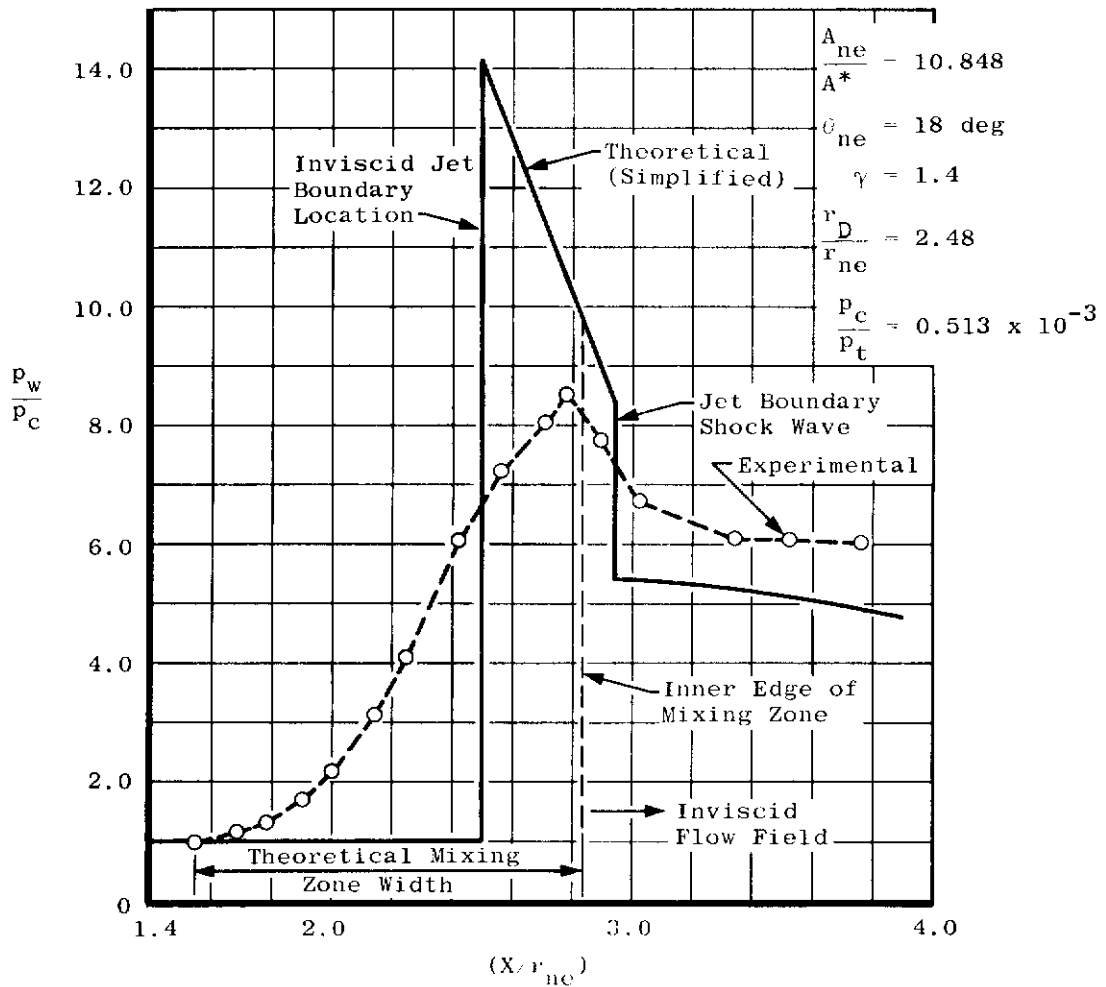


b. Diffuser Wall Static Pressure Distribution

Fig. 10 Theoretical and Experimental Impingement Zone Characteristics

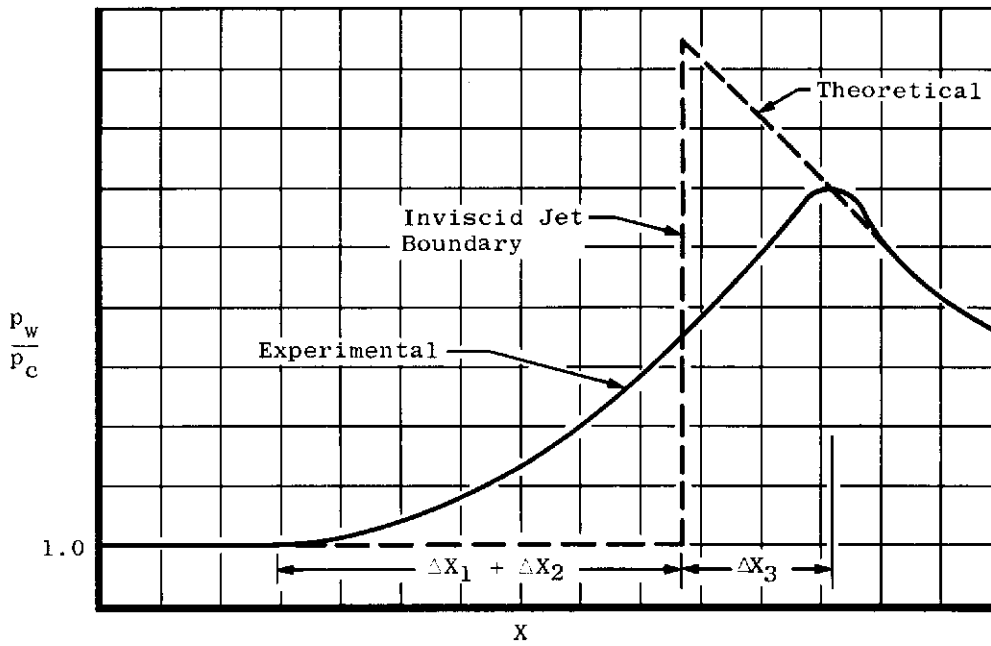


a. Inviscid Flow Conditions

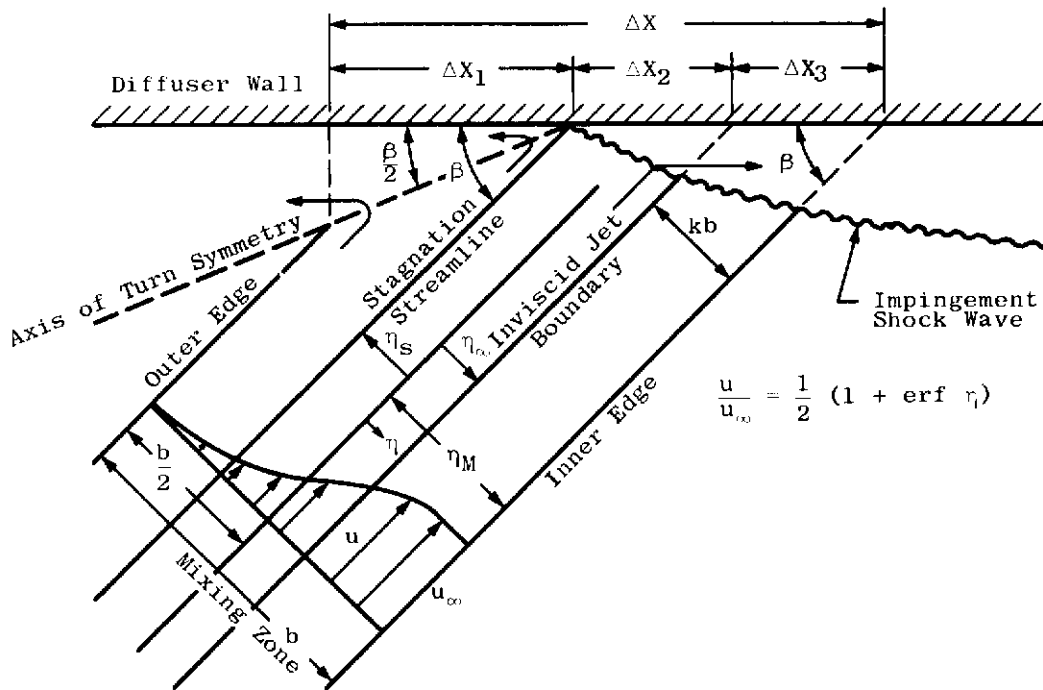


b. Diffuser Wall Static Pressure Distribution

Fig. 11 Theoretical and Experimental Impingement Zone Characteristics



a. Idealized Static Pressure Distribution



$$\frac{u}{u_\infty} = \frac{1}{2} (1 + \text{erf } r_1)$$

b. Idealized Flow Phenomena

Fig. 12 Idealized Flow Phenomena at Impingement Point



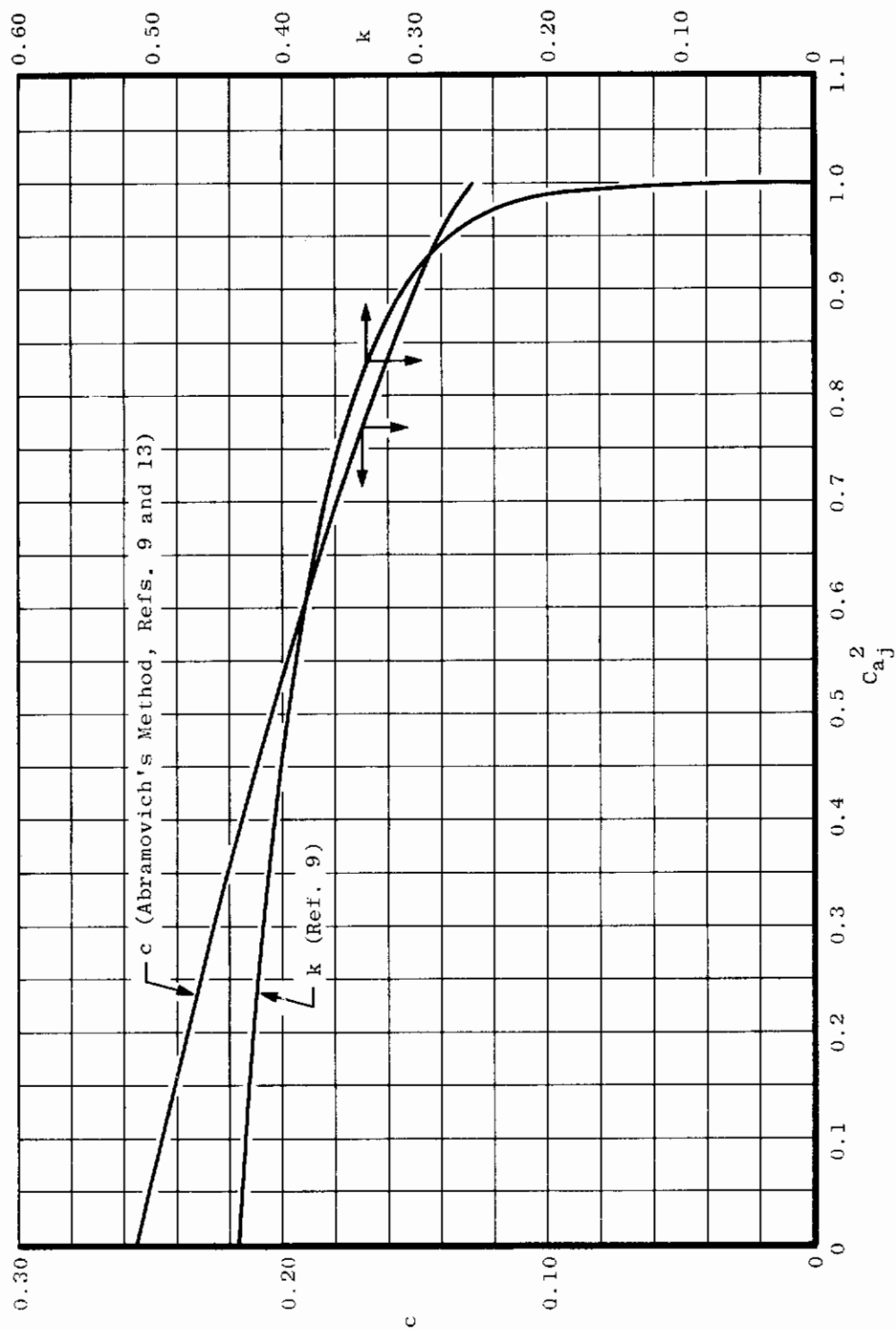
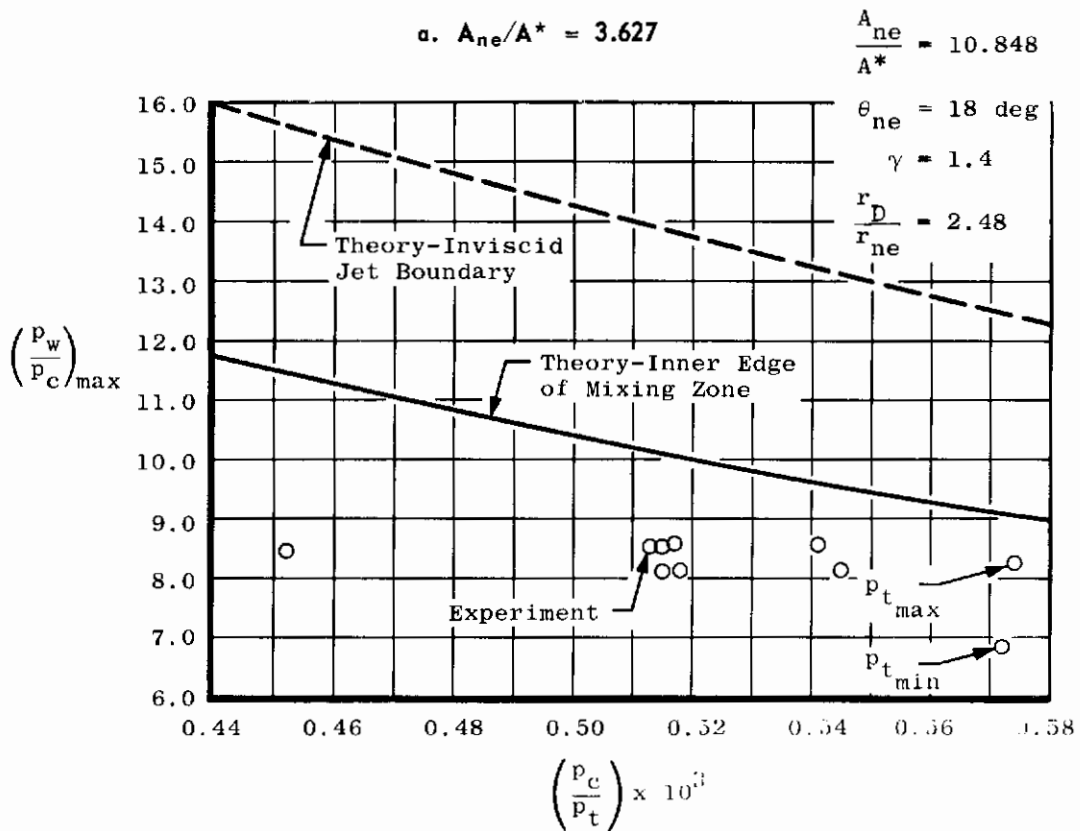
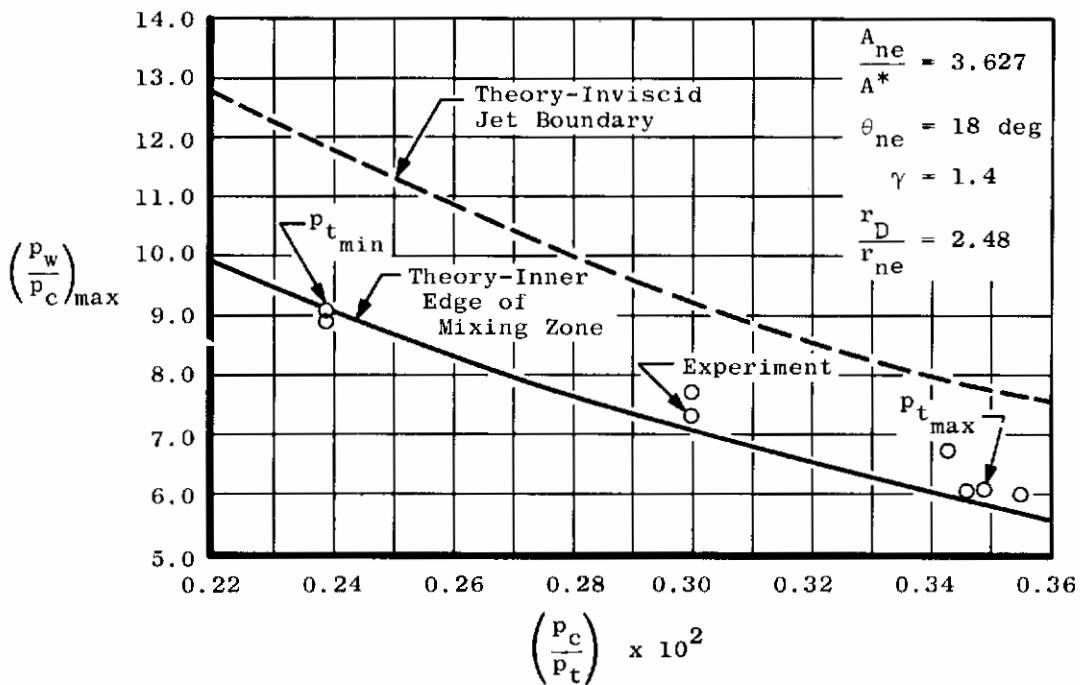
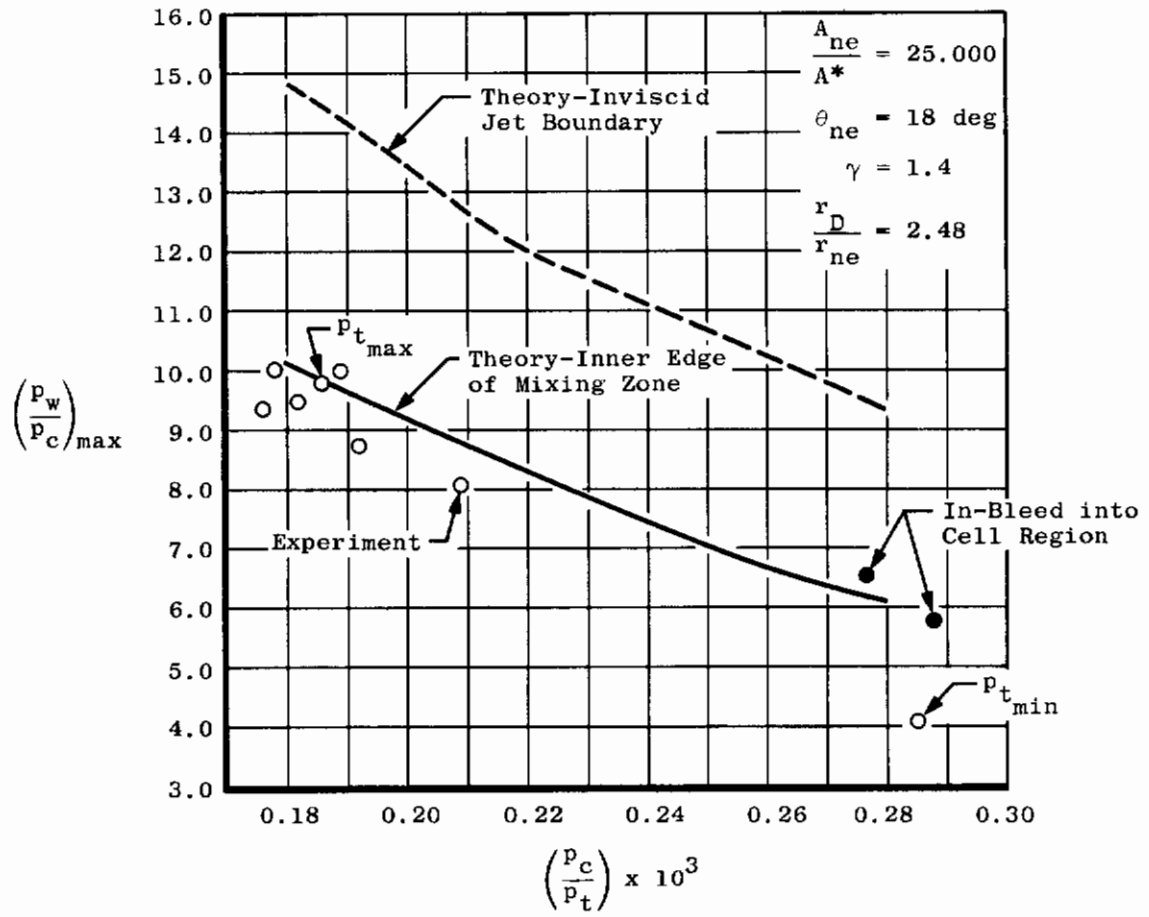


Fig. 13 Variation of Mixing Zone Characteristics with Crocco Number Squared

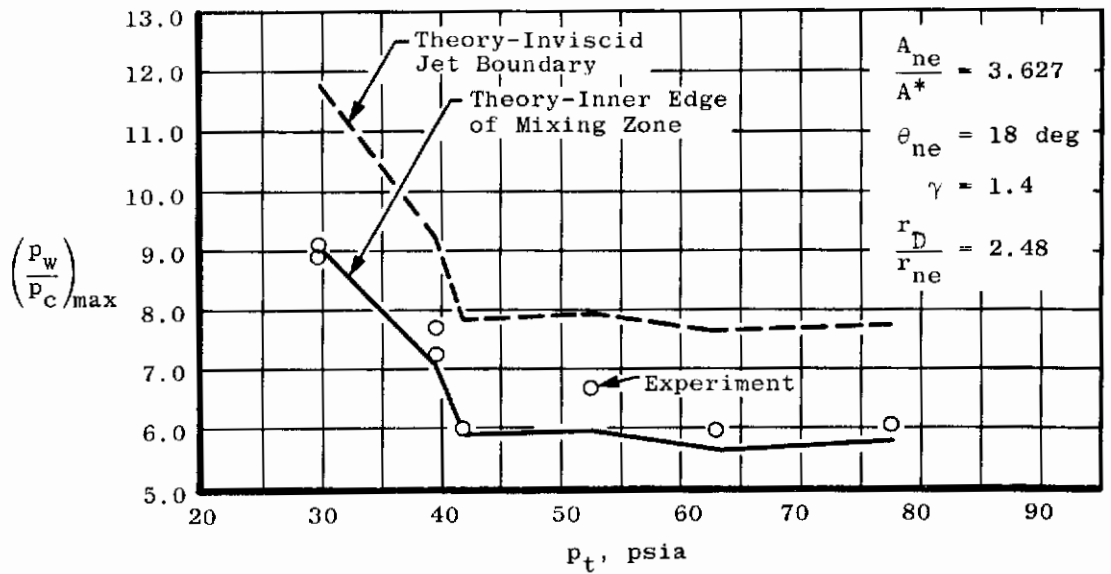


**Fig. 14 Comparison of Theoretical with Experimental Peak Recompression Static Pressure as a Function of  $p_c/p_t$**

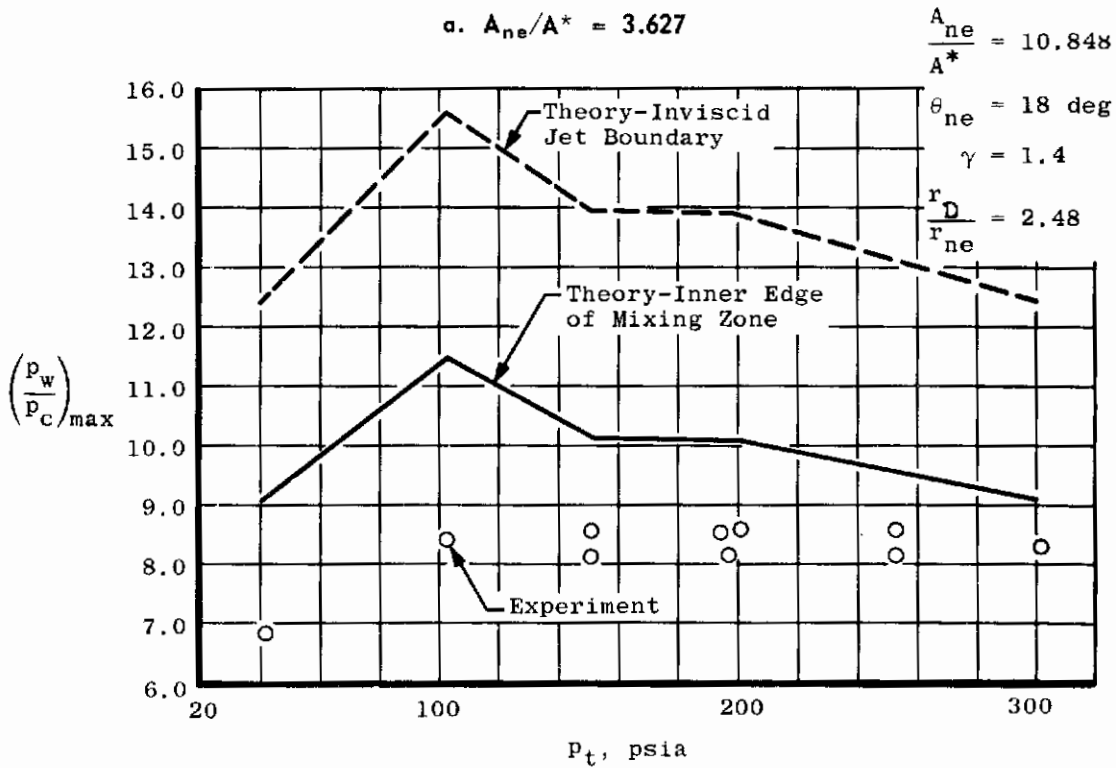


c.  $A_{ne}/A^* = 25.000$

Fig. 14 Concluded



a.  $A_{ne}/A^* = 3.627$



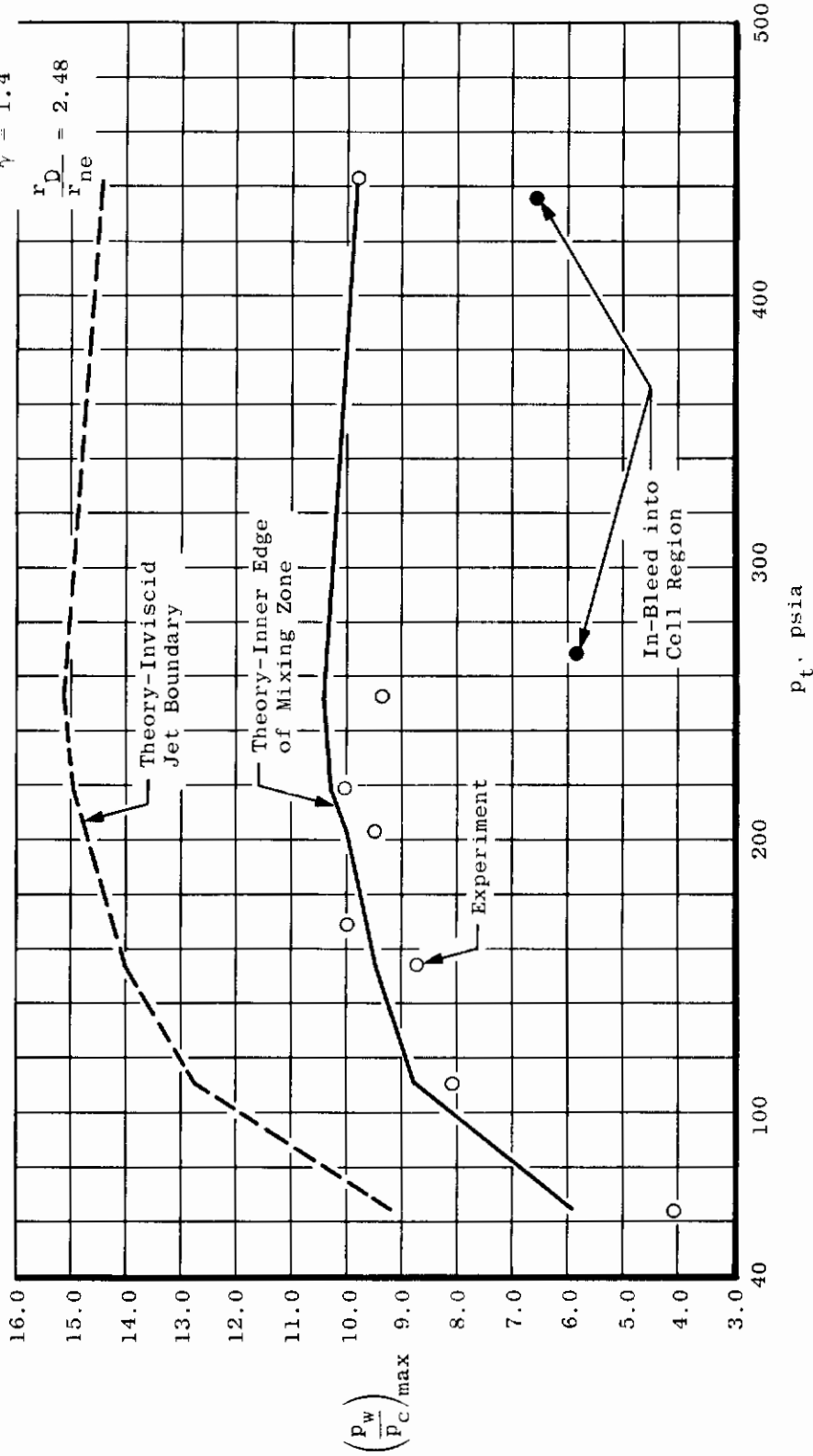
b.  $A_{ne}/A^* = 10.848$

Fig. 15 Comparison of Theoretical with Experimental Peak Recompression Static Pressure as a Function of Nozzle Total Pressure

$\frac{A_{ne}}{A^*} = 25.000$   
 $C_{ne} = 18 \text{ deg}$

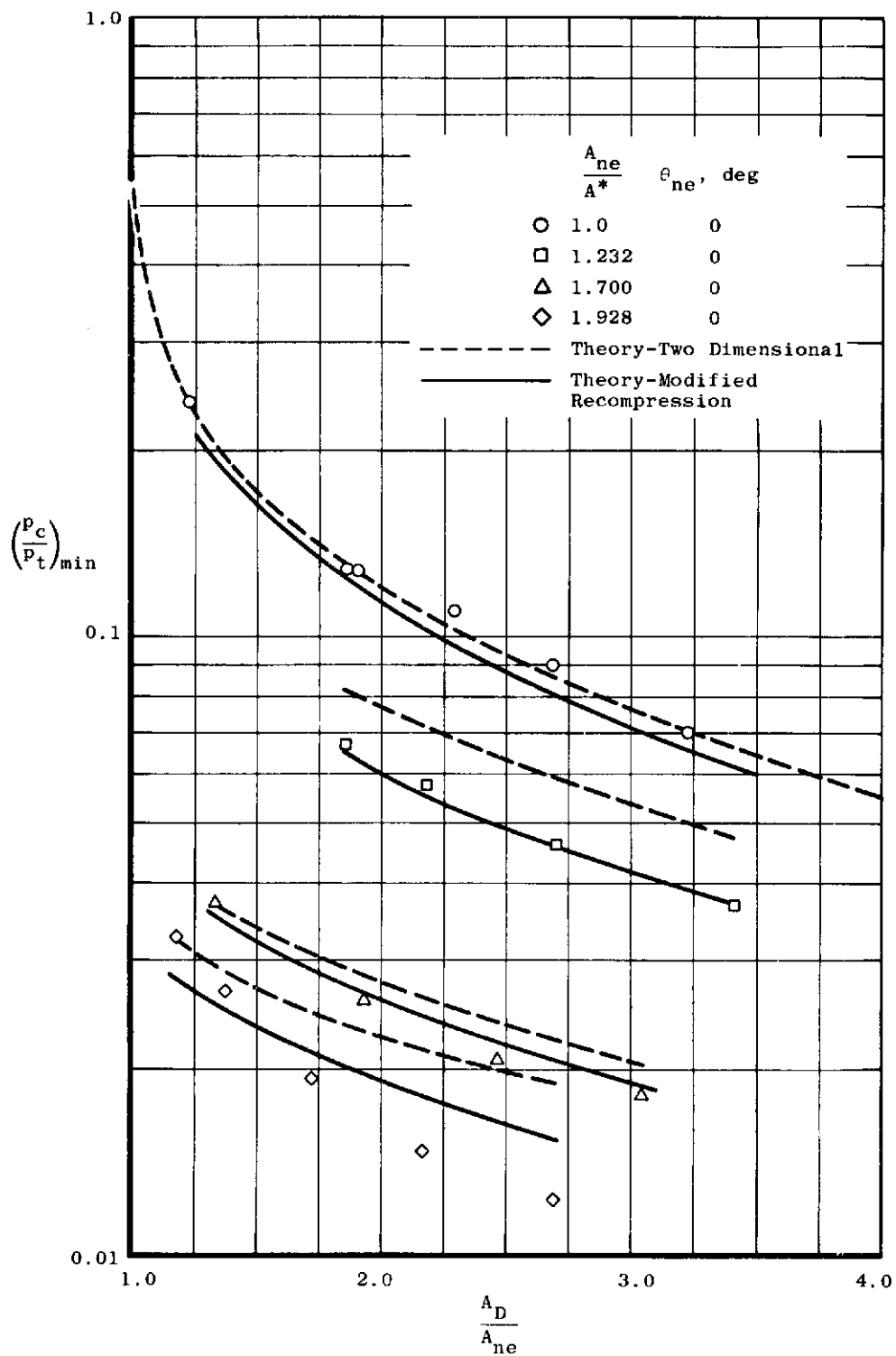
$\gamma = 1.4$

$\frac{r_D}{r_{ne}} = 2.48$



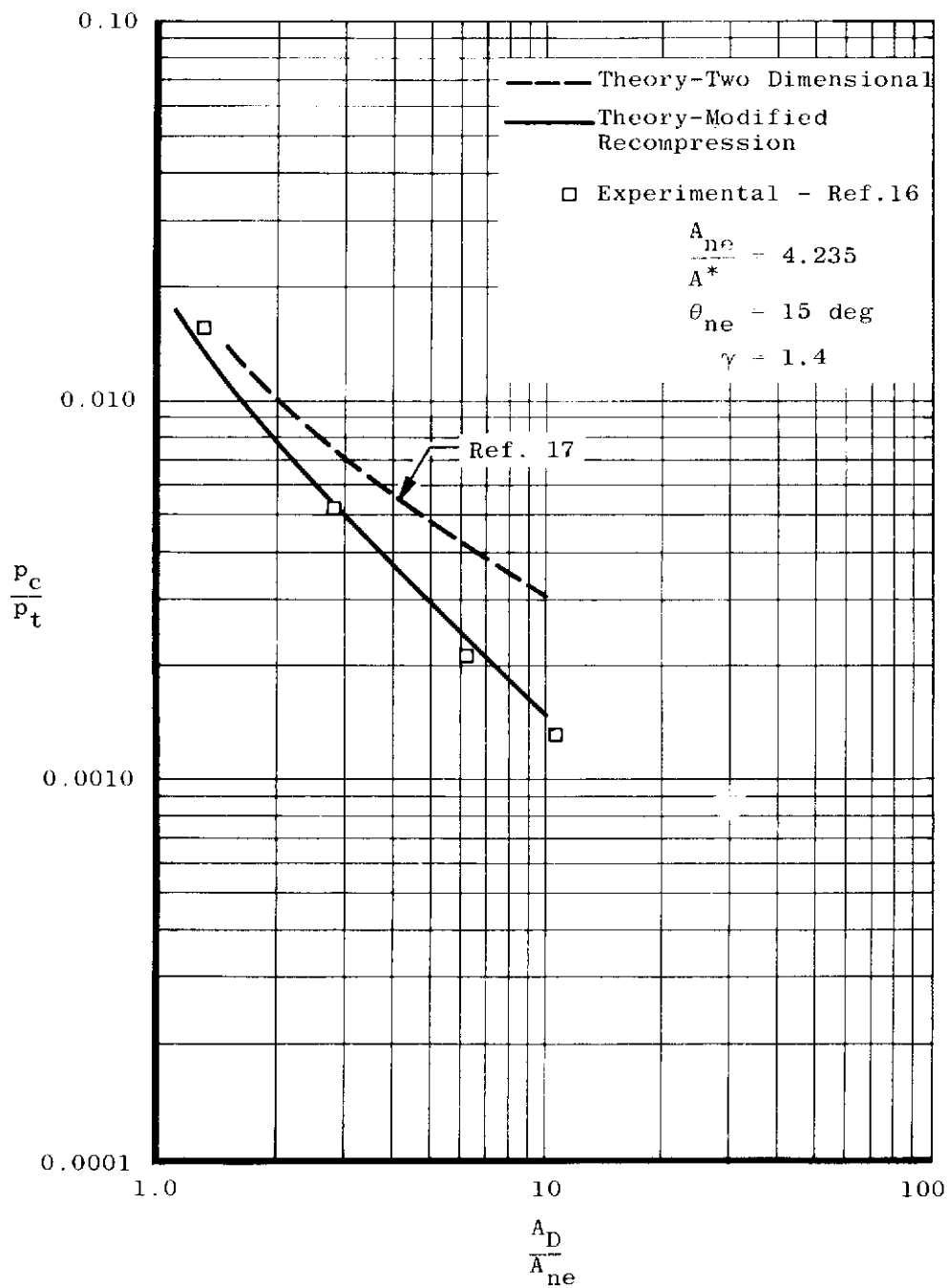
c.  $A_{ne}/A^* = 25.000$

Fig. 15 Concluded



a. Data from Ref. 7

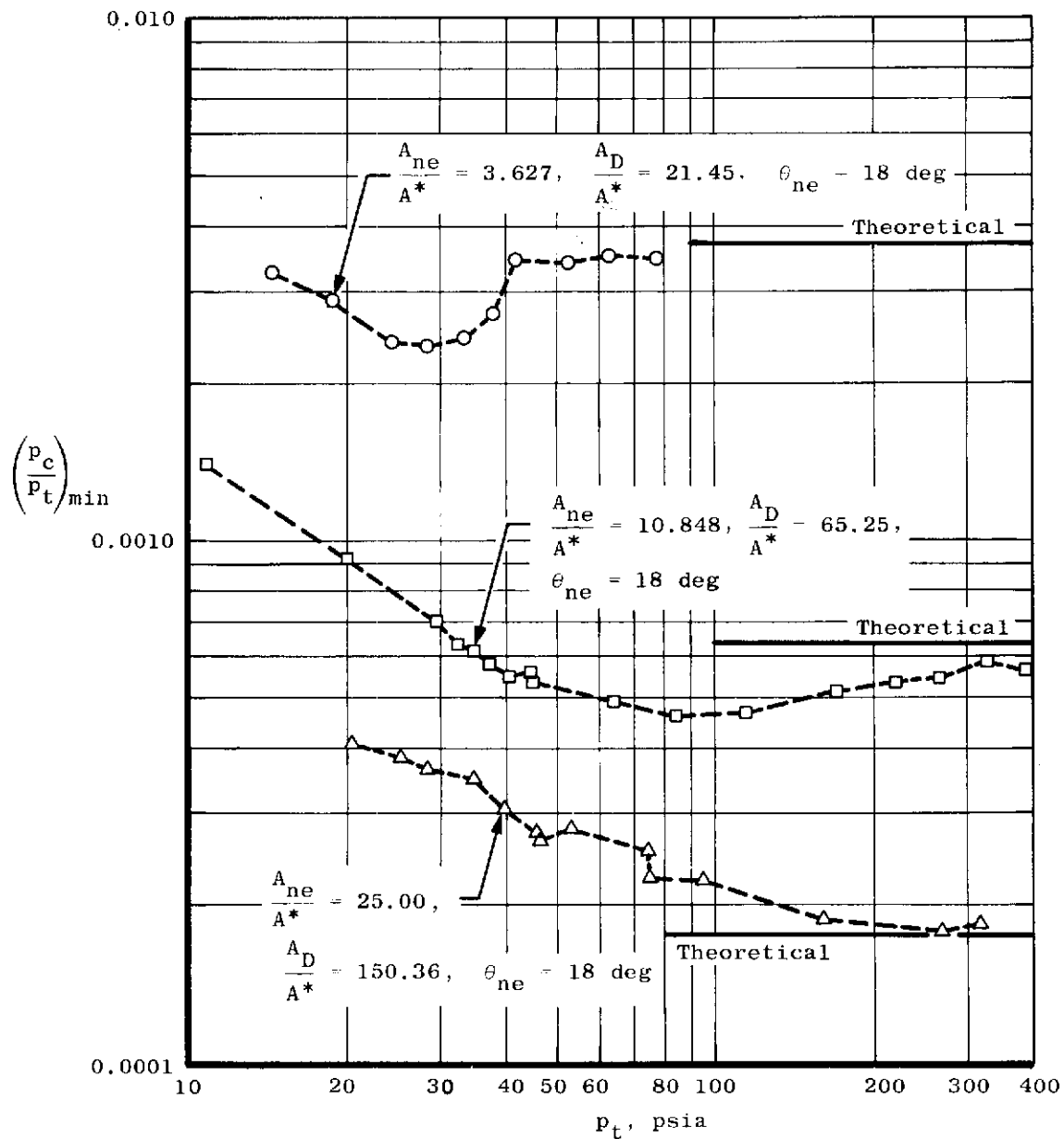
Fig. 16 Comparison of Theoretical with Experimental Minimum Cell Pressure Ratios



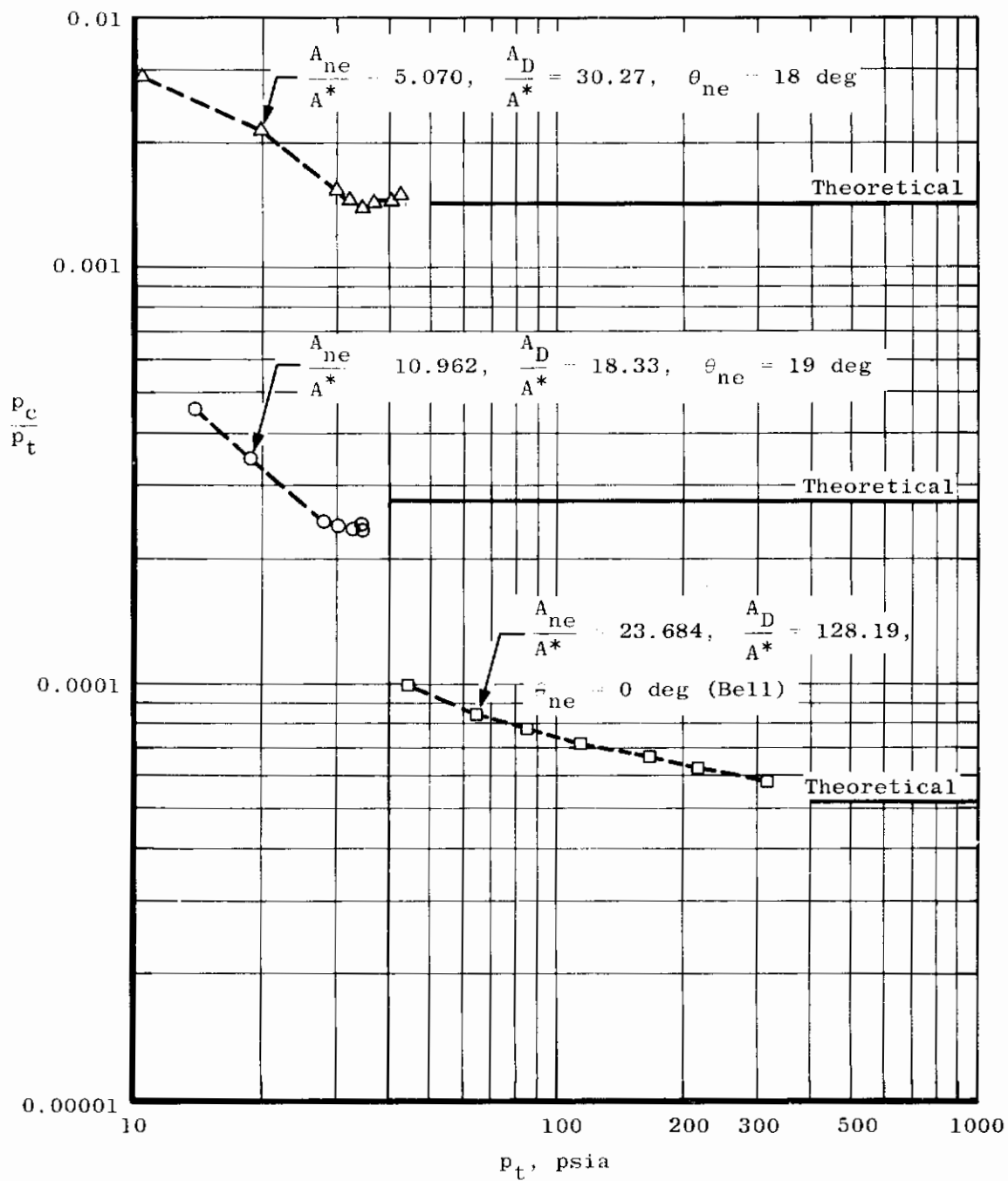
b. Data from Ref. 16

Fig. 16 Continued

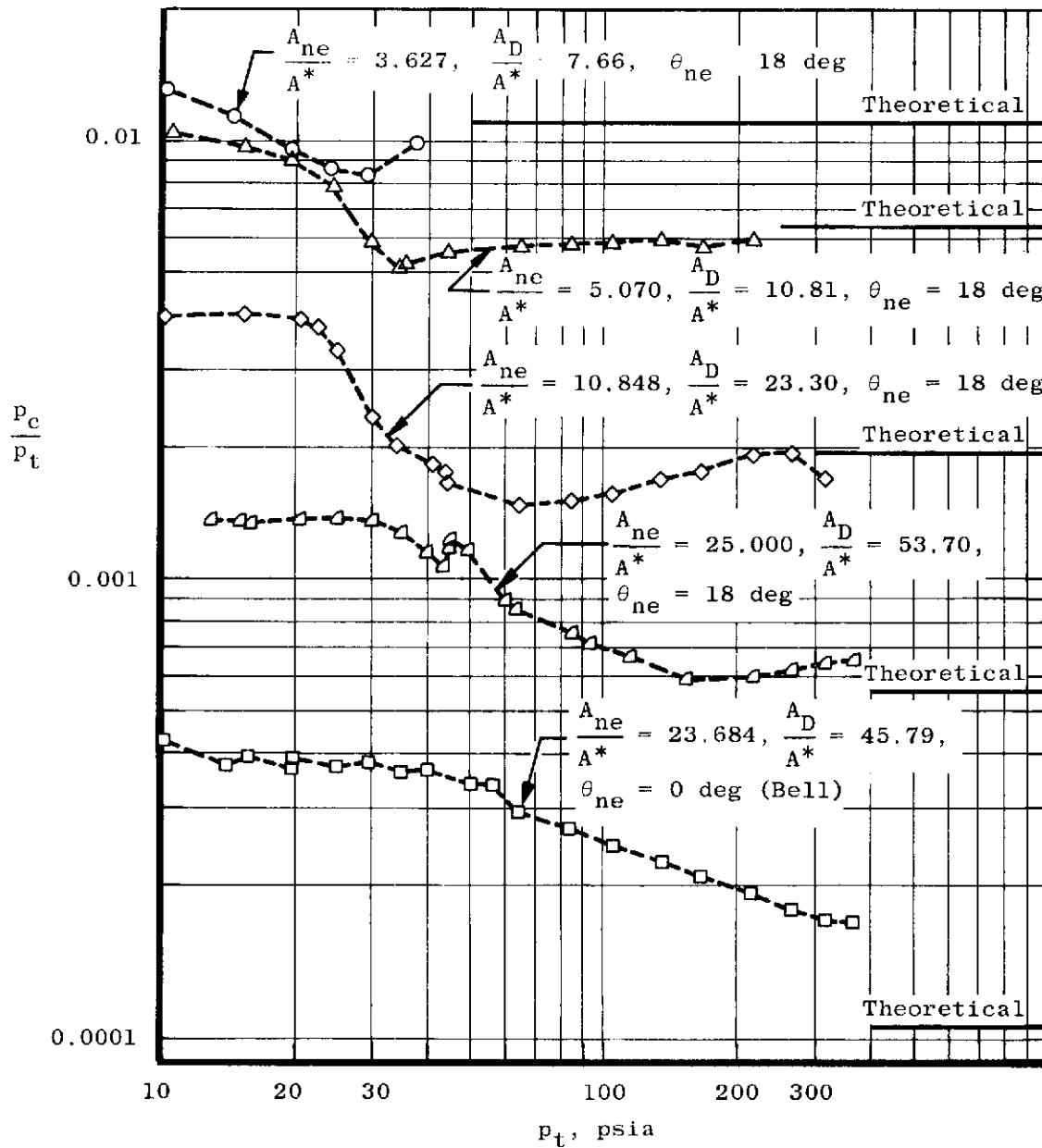




c. Data from Ref. 4  
Fig. 16 Continued



d. Data from Ref. 4  
 Fig. 16 Continued



e. Data from Ref. 4

Fig. 16 Concluded